Journal of Geometry and Physics 112 (2017) 118–146

Contents lists available at ScienceDirect

Journal of Geometry and Physics

journal homepage: www.elsevier.com/locate/jgp

Finsler geometry of nonlinear elastic solids with internal structure

J.D. Clayton *

Courant Institute of Mathematical Sciences[1] *, 503 Warren Weaver Hall, New York, NY 10012, USA*
A. James Clark School, University of Maryland, 2105 J.M. Patterson Building, College Park, MD 20742, USA
Impact Physics Branch, RDRL-WMP-C, US ARL, Aberdeen, MD, 21005-5066, USA

ARTICLE INFO

Article history:
Received 28 April 2016
Accepted 10 November 2016
Available online 19 November 2016

MSC:
51P05
74A05
74A45
74B20

Keywords:
Finsler geometry
Continuum physics
Elasticity
Fracture
Cavitation

ABSTRACT

Concepts from Finsler differential geometry are applied towards a theory of deformable continua with internal structure. The general theory accounts for finite deformation, nonlinear elasticity, and various kinds of structural features in a solid body. The general kinematic structure of the theory includes macroscopic and microscopic displacement fields – i.e., a multiscale representation – whereby the latter are represented mathematically by the director vector of pseudo-Finsler space, not necessarily of unit magnitude. A physically appropriate fundamental (metric) tensor is introduced, leading to affine and nonlinear connections. A deformation gradient tensor is defined via differentiation of the macroscopic motion field, and another metric indicative of strain in the body is a function of this gradient. A total energy functional of strain, referential microscopic coordinates, and horizontal covariant derivatives of the latter is introduced. Variational methods are applied to derive Euler–Lagrange equations and Neumann boundary conditions. The theory is shown to encompass existing continuum physics models such as micromorphic, micropolar, strain gradient, phase field, and conventional nonlinear elasticity models, and it can reduce to such models when certain assumptions on geometry, kinematics, and energy functionals are imposed. The theory is applied to analyze two physical problems in crystalline solids: shear localization/fracture in a two-dimensional body and cavitation in a spherical body. In these examples, a conformal or Weyl-type transformation of the fundamental tensor enables a description of dilatation associated, respectively, with cleavage surface roughness and nucleation of voids or vacancies. For the shear localization problem, the Finsler theory is able to accurately reproduce the surface energy of Griffith's fracture mechanics, and it predicts dilatation-induced toughening as observed in experiments on brittle crystals. For the cavitation problem, the Finsler theory is able to accurately reproduce the vacancy formation energy at a nanoscale resolution, and various solutions describe localized cavitation at the core of the body and/or distributed dilatation and softening associated with amorphization as observed in atomic simulations, with relative stability of solutions depending on the regularization length.

Published by Elsevier B.V.

* Correspondence to: Courant Institute of Mathematical Sciences, 503 Warren Weaver Hall, New York, NY 10012, USA.
E-mail addresses: johnclay@cims.nyu.edu, jdclayt1@umd.edu, john.d.clayton1.civ@mail.mil.

[1] Visiting faculty.

http://dx.doi.org/10.1016/j.geomphys.2016.11.011
0393-0440/Published by Elsevier B.V.

1. Introduction

In Finsler geometry, each point on the base manifold can be envisioned as endowed with a vector of coordinates denoting its position from the origin and a director vector, also referred to herein as an internal state vector, whose components may or may not explicitly depend on position coordinates. Geometric objects such as metric tensors, connections, and derived quantities – e.g., torsion, curvature, and so forth – may in turn depend on both position and direction or internal state. This generality is in contrast to classical Riemannian geometry, wherein ultimate dependence of such geometric objects is on position alone. Finsler geometry encompasses certain geometries of Riemann, Minkowski, and Weyl as special cases. Its generality has resulted in its use in field-theoretical descriptions of nearly all branches of physics: general relativity [1], gravitation [2], quantum mechanics [3], electrodynamics [4], heat conduction [5], and continuum mechanics of solids [6]. The latter topic, i.e., continuum physics of deformable bodies, is of emphasis in the present paper. In this context, fields describing the motion of material particles comprising a body must be introduced along with evolution of the internal state, specifically transformations from referential or Lagrangian coordinates and reference configurational state vectors to spatial or Eulerian coordinates and current configurational state vectors.

Finsler geometry is attributed by name to the doctoral work of P. Finsler nearly a century ago [7]. Early fundamental contributions, including introduction of various connections, were set forth by Cartan [8], Chern [9], and Rund [10]. Modern monographs include [11–13]. Of particular interest here is [14] since it devotes an entire chapter to applications in finite deformation of solids, albeit with content limited to kinematics alone. See also the historical review in [15] – a paper which also advances Finsler geometry via extension of the Cartan–Clifton method of moving frames – and the recent categorization of Finsler connections in [16].

Applications of Finsler geometry in continuum mechanics and physics of deformable solids have been suggested, but not fully developed or realized, since the middle of the 20th century. Amari [17] proposed what appears to be the first Finsler geometric theory of deformation of solids, applied specifically to ferromagnetic elastic–plastic crystals. In this theory, the internal state vector is physically linked to the spin direction of the magnetic moment, and dislocations (a fundamental line defect in crystalline solids [18–20]) are associated with a certain torsion tensor related to anholonomicity [21–23] of the locally relaxed intermediate state of the crystal, following earlier classical differential–geometric treatments by the Japanese school [24]. Kondo [25] briefly discussed how Finsler geometry might be used to describe plastic yielding phenomena. Kröner [26] and Eringen [27] suggested how Finsler geometry may be of potential use for describing mechanics of solids in the context of generalized continuum theories, but did not further develop or expound on these ideas. Around the same time, Ikeda [28,29] developed a theory of deformable media with close connections to Finsler space, again restricted to description of kinematics without consideration of energy functionals or equilibrium equations. Apparently, the application of (pseudo-)Finsler geometry to solid mechanics remained dormant for some 20 years after these suggestions, until appearance of work by Bejancu [14], followed in the next decade by contributions from Saczuk and colleagues [6,30,31]. Herein, a space is designated as pseudo-Finslerian [14,16] rather than strictly Finslerian when a fundamental scalar function with requisite properties [11], from which the metric tensor is obtained by differentiation, does not exist. Theoretical developments again remained scarce for 15 years following, apart from some recent work on anisotropic acoustic wave propagation [32]; for a more comprehensive current literature review, see [33].

It is speculated here that Finsler geometry, in contrast to Riemannian geometry [34–39], has heretofore eluded popularity among mechanicians and physicists due to apparent complexity of calculations, despite its generality and descriptive potential. Indeed, the present author is aware of only one published paper [31] containing solutions to a boundary value problem in Finsler-geometric solid mechanics, and these solutions were obtained numerically rather than analytically and only discussed in brief, though more details are contained in the rather obscure monograph [30] that encompasses [6] and [31]. In the absence of solutions to physically meaningful problems, a complex new theory may offer little advantage or insight over simpler existing methods.

The purpose of this paper is to initiate a new theory of mechanics of deformable solids with microstructure using concepts from Finsler geometry. Many model features, explained as they are introduced, render the present theory distinct from others in the literature [14,31]. The theory is constructed with an aim towards obtaining solutions to pertinent boundary value problems in continuum mechanics, condensed matter physics, and materials physics. Specifically, two problems considered herein are fracture/slip localization in an elastic slab under simple shear (see, e.g., [40] for recent alternative analysis via phase field theory), and cavitation – e.g., void or vacancy formation and expansion – in a spherical elastic domain. The fundamental metric tensor entering the theory in these problems accounts for microscopic dilatation, which is commonplace in fracture of crystalline rocks and minerals [41,42] as well as in the vicinity of point defects (e.g., vacancies, interstitials) and dislocation cores in crystals [18,43,44]. In order to reflect such local volume changes, a Weyl-type rescaling (i.e., a conformal transformation) of the metric tensor is invoked [45,46]. In a novel theory of thermal stresses based on Riemannian geometry, a similar rescaling of a metric tensor on the material manifold was invoked to study isotropic nonlinear elastic solids [47]. Unlike prior theoretical and computational studies in crystal inelasticity [48,49], the present developments do not require a multiplicative decomposition of the deformation gradient into two (or more) terms, but such a treatment is not precluded by the general theory and has been proposed elsewhere in a merging of continuum phase field and Finsler geometric treatments of deformation twinning in crystals [33]. Applications considered herein are also restricted to initially homogeneous bodies, e.g., single crystals or homogenized polycrystals; not considered explicitly are

spatially heterogeneous bodies such as those with varying elastic moduli [48] or varying stress-free strains [50], though the general theory does not preclude analysis of such problems.

This paper is organized as follows. Kinematics and geometry pertinent to a new pseudo-Finsler theory of continuum physics are described in Section 2, including motions at macro- and micro-scales, strain metrics, and differential–geometric objects such as horizontal and vertical connections. An energy functional over the domain is developed in Section 3 that includes dependence on the referential internal state vector and its material gradient, from which Euler–Lagrange equations yield the conservation laws of static equilibrium for incremental boundary value problems. Crucial in derivation of such equations is a version of the divergence theorem first proven by Rund [51] applied here to vector and two-point tensor fields differentiable over a compact region of the material manifold. Following the philosophies shared in other field-theoretical descriptions of continua with internal structure [52,53], the treatment in Sections 2 and 3 is left very general in nature, such that more specific assumptions (e.g., on energy functionals and choices of metric tensors and connections) are introduced later as needed to enable applications to diverse physical problems.

In Section 4, an alternative energy functional is introduced depending on the current configurational internal state and its material gradient. It is explained how this alternative representation encompasses finite deformation micromorphic theory [54] and therefore its subclasses such as micropolar elasticity, linear micromorphic elasticity [55], second gradient nonlinear elasticity, and classical nonlinear hyperelasticity. It is also remarked how the theory (with the energy functional of Section 3) reduces to a variational phase field model [40,56] when a Riemannian metric tensor and classical kinematics are invoked. Further highlighted in discussion of Section 4 are unique features of the present theory in comparison with other models.

Application of the theory towards problems involving shear failure – e.g., dislocation glide, adiabatic shear band formation, or mode II separation – is presented in Section 5. Application towards problems involving cavitation is given in Section 6. In the applications sections, links among geometric objects/parameters entering the theory and physical concepts are highlighted and comparisons with predictions of other classical field approaches are noted. Also emphasized in the discussion are predictive capabilities of the present Finsler geometric theory that cannot be obtained using other known continuum models with a basis in Riemannian geometry. Conclusions follow in Section 7.

2. Pseudo-Finsler geometry and kinematics

Discussed in turn are aspects of the referential – e.g., initial – configuration of the material body, the deformed configuration of the material body, and then the transformations or motions between the two configurations. In the absence of deformation, geometric concepts can be considered standard in the context of generalized (pseudo-)Finsler geometry [10,11,14,16], to which the reader may refer for more details.

2.1. Reference configuration geometry

The reference configuration is identified with a particular instant in time at which a deformable solid body is considered undeformed, following the usual convention of continuum physics [20]. A differential manifold $\mathfrak{M}$ of spatial dimension 3 is then physically identified with a deformable solid body embedded in ambient Euclidean 3-space. Let $X \in \mathfrak{M}$ denote a material point or material particle, and let $\{X^A\}(A = 1, 2, 3)$ denote a coordinate chart that, depending on topology of the material manifold, may partially or completely cover $\mathfrak{M}$. Attached to each point is a vector $\boldsymbol{D}$, or equivalently a chart of secondary coordinates $\{D^A\}(A = 1, 2, 3)$ is assigned that is treated as a field description of structure in the solid and can be associated with a second manifold $\mathfrak{U}$ of dimension 3. Herein, $\boldsymbol{D}$ need not be of unit length. Analogously, $\mathfrak{U}$ may be covered by a single or multiple charts depending on topology. Regarding notation, dependence of a function on (X, D) implies dependence on charts $(\{X^A\}, \{D^A\})$.

Following notation of [14], the description of the reference state of the body can be couched in terms of pseudo-Finsler geometry. Define $\mathcal{Z} = (\mathfrak{Z}, \Pi, \mathfrak{M}, \mathfrak{U})$ as a fiber bundle of total (pseudo-Finsler) space $\mathfrak{Z}$ (dimension 6), where $\Pi : \mathfrak{Z} \to \mathfrak{M}$ is the projection and $\mathfrak{U}$ the fiber. A chart covering a region of $\mathfrak{Z}$ is then $\{X, D\}$. The natural or holonomic basis on $\mathfrak{Z}$ is the field of frames $\{\frac{\partial}{\partial X^A}, \frac{\partial}{\partial D^A}\}$. Coordinate transformations from $\{X, D\}$ to another chart $\{\tilde{X}, \tilde{D}\}$ on $\mathfrak{Z}$ are of the usual Finsler form [11]

$$\tilde{X}^A = \tilde{X}^A(X^1, X^2, X^3), \qquad \tilde{D}^A(X) = Q^A_B(X) D^B. \tag{2.1}$$

Let $Q^A_B = \frac{\partial \tilde{X}^A}{\partial X^B}$. From the chain rule, holonomic basis vectors on $T\mathfrak{Z}$ then transform as [11,14]

$$\frac{\partial}{\partial \tilde{X}^A} = \frac{\partial X^B}{\partial \tilde{X}^A}\frac{\partial}{\partial X^B} + \frac{\partial^2 X^B}{\partial \tilde{X}^A \partial \tilde{X}^C}\tilde{D}^C \frac{\partial}{\partial D^B}, \qquad \frac{\partial}{\partial \tilde{D}^A} = \frac{\partial X^B}{\partial \tilde{X}^A}\frac{\partial}{\partial D^B}. \tag{2.2}$$

Let $N^A_B(X, D)$ denote nonlinear connection coefficients. Non-holonomic basis vectors, which unlike their holonomic counterparts transform as typical vectors, are defined in the usual manner as

$$\frac{\delta}{\delta X^A} = \frac{\partial}{\partial X^A} - N^B_A \frac{\partial}{\partial D^B}, \qquad \delta D^A = dD^A + N^A_B dX^B. \tag{2.3}$$

Noting the scalar products $\langle \frac{\delta}{\delta X^B}, dX^A \rangle = \delta^A_B$ and $\langle \frac{\partial}{\partial D^B}, \delta D^A \rangle = \delta^A_B$, the set $\{\frac{\delta}{\delta X^A}, \frac{\partial}{\partial D^A}\}$ serves as a convenient local basis on $T\mathfrak{Z}$, and the reciprocal set $\{dX^A, \delta D^A\}$ for $T^*\mathfrak{Z}$ [16]. The Sasaki metric tensor [11,57] invokes the latter:

$$\boldsymbol{G}(X, D) = G_{AB}(X, D) dX^A \otimes dX^B + G_{AB}(X, D) \delta D^A \otimes \delta D^B; \tag{2.4}$$

$$G_{AB} = \boldsymbol{G}\left(\frac{\delta}{\delta X^A}, \frac{\delta}{\delta X^B}\right) = \boldsymbol{G}\left(\frac{\partial}{\partial D^A}, \frac{\partial}{\partial D^B}\right). \tag{2.5}$$

Components G_{AB} and their inverse components G^{AB} are used to lower and raise indices in the usual manner, and $G(X, D) = \det[G_{AB}(X, D)]$. Differentiation is hereafter denoted by the following condensed notation:

$$\partial_A(\cdot) = \frac{\partial(\cdot)}{\partial X^A}, \quad \bar{\partial}_A(\cdot) = \frac{\partial(\cdot)}{\partial D^A}; \qquad \delta_A(\cdot) = \frac{\delta(\cdot)}{\delta X^A} = \partial_A(\cdot) - N^B_A \bar{\partial}_B(\cdot). \tag{2.6}$$

Christoffel symbols of the second kind for the Levi-Civita connection on $\mathfrak{M}$ are derived in the usual way:

$$\gamma^A_{BC} = \tfrac{1}{2} G^{AD}(\partial_C G_{BD} + \partial_B G_{CD} - \partial_D G_{BC}) = G^{AD}\gamma_{BCD}. \tag{2.7}$$

Cartan's tensor in the reference configuration is defined as

$$C^A_{BC} = \tfrac{1}{2} G^{AD}(\bar{\partial}_C G_{BD} + \bar{\partial}_B G_{CD} - \bar{\partial}_D G_{BC}) = G^{AD} C_{BCD}. \tag{2.8}$$

Horizontal coefficients of the Chern–Rund and Cartan connections are defined as

$$\Gamma^A_{BC} = \tfrac{1}{2} G^{AD}(\delta_C G_{BD} + \delta_B G_{CD} - \delta_D G_{BC}) = G^{AD}\Gamma_{BCD}. \tag{2.9}$$

Components of the spray and derived nonlinear connection coefficients are, respectively,

$$G^A = \tfrac{1}{2}\gamma^A_{BC} D^B D^C, \qquad G^A_B = \bar{\partial}_B G^A. \tag{2.10}$$

Letting ∇ denote the covariant derivative, horizontal gradients of basis vectors are determined by the generic affine connection coefficients H^A_{BC} and K^A_{BC}:

$$\nabla_{\delta/\delta X^B} \frac{\delta}{\delta X^C} = H^A_{BC} \frac{\delta}{\delta X^A}, \qquad \nabla_{\delta/\delta X^B} \frac{\partial}{\partial D^C} = K^A_{BC} \frac{\partial}{\partial D^A}. \tag{2.11}$$

Vertical gradients are denoted by the generic connection coefficients V^A_{BC} and Y^A_{BC}:

$$\nabla_{\partial/\partial D^B} \frac{\partial}{\partial D^C} = V^A_{BC} \frac{\partial}{\partial D^A}, \qquad \nabla_{\partial/\partial D^B} \frac{\delta}{\delta X^C} = Y^A_{BC} \frac{\delta}{\delta X^A}. \tag{2.12}$$

Developments to this point apply for pseudo-Finsler space or Finsler space. The latter classification holds when a C^∞ fundamental scalar function $\mathfrak{L}(X, D)$ exists at every point of $\mathfrak{U} \setminus 0$, homogeneous of degree one in $\boldsymbol{D}$ [11], from which the metric tensor, spray connection coefficients, and Cartan tensor are derived, the latter with additional symmetry not necessarily present in (2.8):

$$G_{AB} = \tfrac{1}{2}\bar{\partial}_A\bar{\partial}_B(\mathfrak{L}^2), \qquad G^A_B = \gamma^A_{BC} D^C - C^A_{BC}\gamma^C_{DE} D^D D^E = \Gamma^A_{BC} D^C, \qquad C_{ABC} = \tfrac{1}{4}\bar{\partial}_A\bar{\partial}_B\bar{\partial}_C(\mathfrak{L}^2). \tag{2.13}$$

Remark 1. Formally, the Chern–Rund connection is defined when (2.13) holds and $N^A_B = G^A_B, H^A_{BC} = K^A_{BC} = \Gamma^A_{BC}, V^A_{BC} = Y^A_{BC} = 0$; the Cartan connection is defined when (2.13) holds and $N^A_B = G^A_B, H^A_{BC} = K^A_{BC} = \Gamma^A_{BC}, V^A_{BC} = Y^A_{BC} = C^A_{BC}$ [16]. Let $(\cdot)_{|C}$ denote horizontal covariant differentiation in a coordinate chart $\{X^C\}$. Then when either of these connections is used, the horizontal covariant derivative of the metric tensor vanishes:

$$G_{AB|C} = \delta_C G_{AB} - \Gamma^D_{CA} G_{DB} - \Gamma^D_{CB} G_{DA} = \partial_C G_{AB} - N^D_C \bar{\partial}_D G_{AB} - \Gamma^D_{CA} G_{DB} - \Gamma^D_{CB} G_{DA} = 0. \tag{2.14}$$

Remark 2. A (pseudo)-Finsler space degenerates to a Riemannian space when $G_{AB}(X, D) \to G_{AB}(X)$, and to a locally Minkowskian space when $\mathfrak{L}(X, D) \to \mathfrak{L}(D)$ [16].

Let $\mathrm{d}\boldsymbol{X}$ denote a differential line element on $\mathfrak{M}$, and let $\mathrm{d}\boldsymbol{D}$ denote a corresponding element on $\mathfrak{U}$, both with components referred to the non-holonomic basis. Squared lengths of these elements with respect to (2.4) are

$$|\mathrm{d}\boldsymbol{X}|^2 = \langle \mathrm{d}\boldsymbol{X}, \boldsymbol{G}\mathrm{d}\boldsymbol{X} \rangle = G_{AB}\mathrm{d}X^A\mathrm{d}X^B, \qquad |\mathrm{d}\boldsymbol{D}|^2 = \langle \mathrm{d}\boldsymbol{D}, \boldsymbol{G}\mathrm{d}\boldsymbol{D} \rangle = G_{AB}\mathrm{d}D^A\mathrm{d}D^B. \tag{2.15}$$

The traditional scalar volume element and the corresponding volume form of $\mathfrak{M}$ are defined respectively as

$$\mathrm{d}V = \sqrt{G}\mathrm{d}X^1\mathrm{d}X^2\mathrm{d}X^3, \qquad d\Omega = \sqrt{G}\mathrm{d}X^1 \wedge \mathrm{d}X^2 \wedge \mathrm{d}X^3. \tag{2.16}$$

Remark 3. Definitions (2.16) are consistent with those of Rund [51] and apply for elements of $\mathfrak{M}$. Other definitions for volume forms and volume elements exist in the literature [31,58], e.g., those involving wedge products of $\mathrm{d}X^A$ and $\mathrm{d}D^A$ which represent volume forms on $\mathfrak{Z}$.

The area form corresponding to a compact region of $\mathfrak{M}$ is

$$\Omega = \sqrt{B}\mathrm{d}U^1 \wedge \mathrm{d}U^2. \tag{2.17}$$

The embedding of $\partial\mathfrak{M}$ in $\mathfrak{M}$ is represented by the local parametric equations $X^A = X^A(U^\alpha)$ $(\alpha = 1, 2)$, $B^A_\alpha = \frac{\partial X^A}{\partial U^\alpha}$, and $B = \det(B^A_\alpha G_{AB} B^B_\beta)$. See [59] for a comprehensive treatment of surfaces in geometry. The following identities are also noted:

$$\delta_A(\ln\sqrt{G}) = \Gamma^B_{AB}, \qquad (\sqrt{G})_{|A} = \partial_A(\sqrt{G}) - N^B_A\bar{\partial}_B(\sqrt{G}) - \sqrt{G}H^B_{AB}. \tag{2.18}$$

Stokes' theorem in terms of a generic C^1 differentiable form $\boldsymbol{\alpha}$ is

$$\int_{\mathfrak{M}} d\boldsymbol{\alpha} = \oint_{\partial\mathfrak{M}} \boldsymbol{\alpha}. \tag{2.19}$$

Theorem 1 (*Rund, 1975*). *Let $\boldsymbol{\alpha}(X, D) = V^A(X, D)\Omega(X, D)$ be a differentiable 2-form in (2.19), and let V^A be contravariant components of vector field $\boldsymbol{V} = V^A\frac{\delta}{\delta X^A}$. Let the horizontal connection be such that the second of (2.18) vanishes, i.e., $H^B_{AB} = \Gamma^B_{AB} \to (\sqrt{G})_{|A} = 0$, and assume that functional relations $D = D(X)$ exist for representation of the internal state at each point $X \in \mathfrak{M}$. Then in a coordinate chart $\{X^A\}$, (2.19) is explicitly*

$$\int_{\mathfrak{M}} [V^A_{|A} + (V^A C^C_{BC} + \bar{\partial}_B V^A)D^B_{;A}]d\Omega = \oint_{\partial\mathfrak{M}} V^A N_A \Omega \tag{2.20}$$

where N_A is the unit outward normal on $\partial\mathfrak{M}$, $V^A_{|A} = \delta_A V^A + V^A H^B_{BA}$, and $D^B_{;A} = \partial_A D^B + N^B_A$.

Proof. Derived and presented by H. Rund in [51].

2.2. Deformed configuration geometry

The current configuration is identified with a particular instant in time at which a solid body is considered deformed. The present discussion fully parallels that of Section 2.1, but with an adjustment in notation for deformed coordinates and their indices, etc., which are denoted via lower-case rather than capital fonts. A differential manifold $\mathfrak{m}$ of spatial dimension 3 is identified with a deformed solid body embedded in ambient Euclidean 3-space. Let $x \in \mathfrak{m}$ denote a spatial point, and let $\{x^a\}(a = 1, 2, 3)$ denote a coordinate chart on $\mathfrak{m}$. Attached to each point is a vector $\boldsymbol{d}$, or equivalently a chart of secondary coordinates $\{d^a\}(a = 1, 2, 3)$ is assigned that is treated as a field description of microstructure and can be associated with a second manifold $\mathfrak{u}$ of dimension 3. Herein, $\boldsymbol{d}$ need not be of unit length.

Again following notation of [14], the deformed state of the body can be couched in terms of pseudo-Finsler geometry. Define $\mathfrak{z} = (\mathfrak{z}, \pi, \mathfrak{m}, \mathfrak{u})$ as a fiber bundle of total (pseudo-Finsler) space $\mathfrak{z}$ (dimension 6), where $\pi : \mathfrak{z} \to \mathfrak{m}$ is the projection and $\mathfrak{u}$ the fiber. A chart covering $\mathfrak{z}$ is $\{x, d\}$. The natural/holonomic basis on $\mathfrak{z}$ is $\{\frac{\partial}{\partial x^a}, \frac{\partial}{\partial d^a}\}$. Coordinate transformations from $\{x, d\}$ to another chart $\{\tilde{x}, \tilde{d}\}$ are

$$\tilde{x}^a = \tilde{x}^a(x^1, x^2, x^3), \qquad \tilde{d}^a(x) = q^a_b(X)d^b. \tag{2.21}$$

Letting $q^a_b = \frac{\partial\tilde{x}^a}{\partial x^b}$, holonomic basis vectors on $T\mathfrak{z}$ transform as

$$\frac{\partial}{\partial\tilde{x}^a} = \frac{\partial x^b}{\partial\tilde{x}^a}\frac{\partial}{\partial x^b} + \frac{\partial^2 x^b}{\partial\tilde{x}^a\partial\tilde{x}^c}\tilde{d}^c\frac{\partial}{\partial d^b}, \qquad \frac{\partial}{\partial\tilde{d}^a} = \frac{\partial x^b}{\partial\tilde{x}^a}\frac{\partial}{\partial d^b}. \tag{2.22}$$

Let $n^a_b(x, d)$ denote nonlinear connection coefficients. Non-holonomic basis vectors are

$$\frac{\delta}{\delta x^a} = \frac{\partial}{\partial x^a} - n^b_a\frac{\partial}{\partial d^b}, \qquad \delta d^a = dd^a + n^a_b dx^b. \tag{2.23}$$

The set $\{\frac{\delta}{\delta x^a}, \frac{\partial}{\partial d^a}\}$ serves as a convenient local basis on $T\mathfrak{z}$, and $\{dx^a, \delta d^a\}$ for $T^*\mathfrak{z}$. The Sasaki metric tensor in spatial coordinates is

$$\boldsymbol{g}(x, d) = g_{ab}(x, d)dx^a \otimes dx^b + g_{ab}(x, d)\delta d^a \otimes \delta d^b; \tag{2.24}$$

$$g_{ab} = \boldsymbol{g}\left(\frac{\delta}{\delta x^a}, \frac{\delta}{\delta x^b}\right) = \boldsymbol{g}\left(\frac{\partial}{\partial d^a}, \frac{\partial}{\partial d^b}\right). \tag{2.25}$$

Components g_{ab} and inverse components g^{ab} are used to lower and raise indices, and $g(x, d) = \det[g_{ab}(x, d)]$. Spatial differentiation is written in condensed form as

$$\partial_a(\cdot) = \frac{\partial(\cdot)}{\partial x^a}, \quad \bar{\partial}_a(\cdot) = \frac{\partial(\cdot)}{\partial d^a}; \qquad \delta_a(\cdot) = \frac{\delta(\cdot)}{\delta x^a} = \partial_a(\cdot) - n^b_a\bar{\partial}_b(\cdot). \tag{2.26}$$

Christoffel symbols of the second kind for the Levi-Civita connection on $\mathfrak{m}$ are

$$\gamma^a_{bc} = \tfrac{1}{2}g^{ad}(\partial_c g_{bd} + \partial_b g_{cd} - \partial_d g_{bc}) = g^{ad}\gamma_{bcd}. \tag{2.27}$$

Cartan's tensor in the current configuration is defined as

$$C^a_{bc} = \tfrac{1}{2}g^{ad}(\bar{\partial}_c g_{bd} + \bar{\partial}_b g_{cd} - \bar{\partial}_d g_{bc}) = g^{ad}C_{bcd}. \tag{2.28}$$

Horizontal coefficients of the spatial Chern–Rund and Cartan connections are

$$\Gamma^a_{bc} = \tfrac{1}{2}g^{ad}(\delta_c g_{bd} + \delta_b g_{cd} - \delta_d g_{bc}) = g^{ad}\Gamma_{bcd}. \tag{2.29}$$

Spatial components of the spray and derived nonlinear connection coefficients are, respectively,

$$g^a = \tfrac{1}{2}\gamma^a_{bc}d^b d^c, \qquad g^a_b = \bar{\partial}_b g^a. \tag{2.30}$$

Letting ∇ denote the covariant derivative, horizontal gradients of basis vectors are determined by the generic affine connection coefficients H^a_{bc} and K^a_{bc}:

$$\nabla_{\delta/\delta x^b}\frac{\delta}{\delta x^c} = H^a_{bc}\frac{\delta}{\delta x^a}, \qquad \nabla_{\delta/\delta x^b}\frac{\partial}{\partial d^c} = K^a_{bc}\frac{\partial}{\partial d^a}. \tag{2.31}$$

Vertical gradients are denoted by the generic connection coefficients V^a_{bc} and Y^a_{bc}:

$$\nabla_{\partial/\partial d^b}\frac{\partial}{\partial d^c} = V^a_{bc}\frac{\partial}{\partial d^a}, \qquad \nabla_{\partial/\partial d^b}\frac{\delta}{\delta x^c} = Y^a_{bc}\frac{\delta}{\delta x^a}. \tag{2.32}$$

Remark 4. The spatial configuration correlates with Finsler rather than pseudo-Finsler space when a C^∞ fundamental scalar function $\mathfrak{l}(x, d)$ exists at every point of $\mathfrak{u} \setminus 0$, homogeneous of degree one in $\boldsymbol{d}$, from which

$$g_{ab} = \tfrac{1}{2}\bar{\partial}_a\bar{\partial}_b(\mathfrak{l}^2), \qquad g^a_b = \gamma^a_{bc}d^c - C^a_{bc}\gamma^c_{de}d^d d^e = \Gamma^a_{bc}d^c, \qquad C_{abc} = \tfrac{1}{4}\bar{\partial}_a\bar{\partial}_b\bar{\partial}_c(\mathfrak{l}^2). \tag{2.33}$$

Remark 5. The Chern–Rund connection is invoked when (2.33) holds and $n^a_b = g^a_b, H^a_{bc} = K^a_{bc} = \Gamma^a_{bc}, V^a_{bc} = Y^a_{bc} = 0$; the Cartan connection is invoked when (2.33) holds and $n^a_b = g^a_b, H^a_{bc} = K^a_{bc} = \Gamma^a_{bc}, V^a_{bc} = Y^a_{bc} = C^a_{bc}$. Let $(\cdot)_{|c}$ denote horizontal covariant differentiation in a spatial chart $\{x^c\}$. Then when either of these connections is used, the horizontal covariant derivative of $\boldsymbol{g}$ vanishes:

$$g_{ab|c} = \delta_c g_{ab} - \Gamma^d_{ca}g_{db} - \Gamma^d_{cb}g_{da} = \partial_c g_{ab} - n^d_c\bar{\partial}_d g_{ab} - \Gamma^d_{ca}g_{db} - \Gamma^d_{cb}g_{da} = 0. \tag{2.34}$$

Remark 6. A (pseudo)-Finsler space degenerates to a Riemannian space when $g_{ab}(x, d) \to g_{ab}(x)$, and to a locally Minkowskian space when $\mathfrak{l}(x, d) \to \mathfrak{l}(d)$.

Let $\mathrm{d}\boldsymbol{x}$ denote a differential line element on $\mathfrak{m}$ and $\mathrm{d}\boldsymbol{d}$ denote a corresponding element on $\mathfrak{u}$. Squared lengths of these elements with respect to (2.24) are

$$|\mathrm{d}\boldsymbol{x}|^2 = \langle \mathrm{d}\boldsymbol{x}, \boldsymbol{g}\,\mathrm{d}\boldsymbol{x}\rangle = g_{ab}\mathrm{d}x^a\mathrm{d}x^b, \qquad |\mathrm{d}\boldsymbol{d}|^2 = \langle \mathrm{d}\boldsymbol{d}, \boldsymbol{g}\,\mathrm{d}\boldsymbol{d}\rangle = g_{ab}\mathrm{d}d^a\mathrm{d}d^b. \tag{2.35}$$

The scalar volume element and volume form of $\mathfrak{m}$ are

$$\mathrm{d}v = \sqrt{g}\mathrm{d}x^1\mathrm{d}x^2\mathrm{d}x^3, \qquad d\omega = \sqrt{g}\mathrm{d}x^1 \wedge \mathrm{d}x^2 \wedge \mathrm{d}x^3. \tag{2.36}$$

Similar to discussion in Remark 3, such elements apply for regions of $\mathfrak{m}$; different definitions [31,58] would be used for elements/forms on $\mathfrak{z}$. By a simple change of notation from referential to spatial quantities, an area form ω can be introduced analogously to Ω in (2.17), as can spatial versions of the coordinate-free Stokes' theorem in (2.19) and Rund's horizontal divergence theorem in (2.20).

2.3. Deformation kinematics

Transformations from referential to spatial coordinates ($\mathfrak{M}$ to $\mathfrak{m}$) and vice versa are denoted by the C^2 functions

$$x^a(X, D) = \varphi^a[X, D(X)], \qquad X^A(x, d) = \Phi^A[x, d(x)]. \tag{2.37}$$

Since the present theory is quasi-static, time does not enter such functions as an explicit independent variable.

Remark 7. Incorporation of the internal state (D or d) in these motion functions distinguishes Finsler kinematics [14,31] from the usual kinematics in Riemannian geometry of classical continuum physics [23,60].

State vector mappings are of the affine form [14]

$$d^a(X,D) = \vartheta^a[X,D(X)] = \vartheta^a_B(X)D^B, \qquad D^A(x,d) = \Theta^A[x,d(x)] = \Theta^A_b(x)d^b. \tag{2.38}$$

The deformation gradient from reference to current (pseudo)-Finsler tangent spaces is defined as

$$\boldsymbol{F}(X,D) = F^a_A(X,D)\frac{\delta}{\delta x^a}\otimes dX^A = \frac{\partial\varphi^a(X,D)}{\partial X^A}\frac{\delta}{\delta x^a}\otimes dX^A = \frac{\partial \boldsymbol{x}(X,D)}{\partial \boldsymbol{X}}, \qquad F^a_A = \partial_A x^a. \tag{2.39}$$

The analogous mapping from spatial to referential tangent spaces is the two-point tensor

$$\boldsymbol{f}(x,d) = f^A_a(x,d)\frac{\delta}{\delta X^A}\otimes dx^a = \frac{\partial\Phi^A(x,d)}{\partial x^a}\frac{\delta}{\delta X^A}\otimes dx^a = \frac{\partial \boldsymbol{X}(x,d)}{\partial \boldsymbol{x}}, \qquad f^A_a = \partial_a X^A. \tag{2.40}$$

Deformation gradients $\boldsymbol{F}$ and $\boldsymbol{f}$ are presumed invertible with positive determinants, and are mutual inverses of each other at coincident points on $\mathfrak{M}$ or $\mathfrak{m}$:

$$F^a_A[X,D(X)]f^A_b[x(X,D),d(x(X,D))] = \delta^a_b, \qquad f^A_a[x,d(x)]F^a_B[X(x,d),D(X(x,d))] = \delta^A_B. \tag{2.41}$$

Remark 8. Components of $\boldsymbol{F}$ and $\boldsymbol{f}$ are defined in an identical fashion by Bejancu [12]. Tensor definitions (2.39) and (2.40) potentially differ in two ways from their counterparts in Riemannian geometry:

- Components F^a_A and f^A_a functionally depend on internal state (D or d) as well as position of point X or x;
- Basis vectors corresponding to the first (contravariant) leg of each tensor are generally non-holonomic. This enables configurational transformations (i.e., push-forwards and pull-backs) of vectors and tensors to be calculated in a completely analogous fashion to transformations between different coordinate charts in the same configuration.

Transformation equations for differential line elements follow by generalizing fundamental postulates of continuum mechanics in Riemannian space [23,60] to account for the non-holonomic bases of Finsler space:

$$\mathrm{d}\boldsymbol{x} = \frac{\partial \boldsymbol{x}}{\partial \boldsymbol{X}}\mathrm{d}\boldsymbol{X} \Leftrightarrow \mathrm{d}x^a = F^a_A\mathrm{d}X^A, \qquad \mathrm{d}\boldsymbol{X} = \frac{\partial \boldsymbol{X}}{\partial \boldsymbol{x}}\mathrm{d}\boldsymbol{x} \Leftrightarrow \mathrm{d}X^A = f^A_a\mathrm{d}x^a. \tag{2.42}$$

Applying (2.42) and invoking definitions of the determinant and (2.16) and (2.36), volume elements and volume forms transform between reference and spatial frames on $\mathfrak{M}$ and $\mathfrak{m}$ as

$$\mathrm{d}v = J\mathrm{d}V = [\det(F^a_A)\sqrt{g/G}]\mathrm{d}V, \quad \mathrm{d}V = j\mathrm{d}v = [\det(f^A_a)\sqrt{G/g}]\mathrm{d}v; \qquad d\omega = Jd\Omega, \quad d\Omega = jd\omega. \tag{2.43}$$

Lengths of deformed and initial line elements can be compared using the deformation tensor $\boldsymbol{C}$:

$$|\mathrm{d}\boldsymbol{x}|^2 = F^a_A F^b_B g_{ab}\mathrm{d}X^A\mathrm{d}X^B = C_{AB}\mathrm{d}X^A\mathrm{d}X^B = \langle \mathrm{d}\boldsymbol{X}, \boldsymbol{C}\mathrm{d}\boldsymbol{X}\rangle, \qquad \boldsymbol{C} = C_{AB}dX^A\otimes dX^B = F^a_A g_{ab}F^b_B dX^A\otimes dX^B. \tag{2.44}$$

It follows that $\det(C_{AB}) = J^2G$. For the directors or state vectors, a similar construction using (2.38) gives

$$|\boldsymbol{d}|^2 = \vartheta^a\vartheta_a = \Xi_{AB}D^AD^B = \langle \boldsymbol{D}, \boldsymbol{\Xi D}\rangle, \qquad \boldsymbol{\Xi} = \Xi_{AB}\delta D^A\otimes\delta D^B = \vartheta^a_A g_{ab}\vartheta^b_B\delta D^A\otimes\delta D^B. \tag{2.45}$$

Theorem 2. *The transformation rule for gradients of non-holonomic bases is*

$$\nabla_{\delta/\delta X^A}\frac{\delta}{\delta x^c} = (F^a_A - N^B_A\bar{\partial}_B x^a)H^b_{ac}\frac{\delta}{\delta x^b}. \tag{2.46}$$

Proof. Applying definitions (2.39), (2.31), and (2.23) successively,

$$\nabla_{\delta/\delta X^A}\frac{\delta}{\delta x^c} = \frac{\delta x^a}{\delta X^A}\nabla_{\delta/\delta x^a}\frac{\delta}{\delta x^c} = \delta_A\varphi^a H^b_{ac}\frac{\delta}{\delta x^b} = (F^a_A - N^B_A\bar{\partial}_B x^a)H^b_{ac}\frac{\delta}{\delta x^b}. \tag{2.47}$$

Remark 9. It is emphasized that (2.43)–(2.46) are derived from (2.42) and prior definitions and thus are not independent theoretical assumptions.

Remark 10. Definitions (2.39) and (2.40), also used by Bejancu [14], are thought to be the simplest and most convenient possible choices that reduce to their classical counterparts when kinematics are Riemannian rather than Finslerian. Other more complex definitions for the deformation gradient in Finsler-type continuum mechanics have been posited, e.g., covariant derivatives in [30,31]. The rationale for introduction of more complicated definitions/assumptions on Finsler kinematics is unclear and does not appear to be physically necessary.

Remark 11. Material in Sections 2.1 and 2.2 can be considered standard in the context of (pseudo-)Finsler geometry [10,11,14,16]. On the other hand, content of Section 2.3 is not addressed in most monographs on pure Finsler geometry. Kinematic assumptions in a few other historic works merit mention. In [17], an equation of the form $\mathrm{d}x^a = F^a_A\mathrm{d}X^A$ is used, where $F^a_A = F^a_A(X,D)$ in general, with the multiplicative form $F^a_A(X,D) = A^a_\beta(X)B^\beta_A(D)$ considered in one example. This work [17] omits the contributions of components of Cartan's tensor and nonlinear connection coefficients in (2.20) when applying the divergence theorem on the material manifold to derive balance laws. In [29], an equation of the form $\mathrm{d}x^a = F^a_A\mathrm{d}X^A$ is used, but no explicit definition is provided for components F^a_A, which presumably could depend on both position and direction.

3. Energy functional and conservation laws

The following variational principle is set forth, where Ψ is the action integral for a closed and simply connected region of $\mathfrak{M}$ with boundary $\partial\mathfrak{M}$, and surface forces are $\boldsymbol{p} = p_a dx^a$, a mechanical load vector (force per unit reference area), and $\boldsymbol{z} = z_A \delta D^A$, a thermodynamic force conjugate to the internal state vector:

$$\delta\Psi(\boldsymbol{\varphi}, \boldsymbol{D}) = \oint_{\partial\mathfrak{M}} (\langle \boldsymbol{p}, \delta\boldsymbol{x}\rangle + \langle \boldsymbol{z}, \delta\boldsymbol{D}\rangle)\Omega. \tag{3.1}$$

Letting ψ denote potential energy density, i.e., internal or free energy density in the absence of explicit kinetic and thermal effects, this becomes

$$\delta \int_{\mathfrak{M}} \psi d\Omega = \oint_{\partial\mathfrak{M}} [p_a \delta x^a + z_A \delta(D^A)]\Omega, \tag{3.2}$$

where the first variation of $\boldsymbol{D}$ is enclosed in parentheses to avoid confusion with basis vector δD^A. The following functional form of the energy density per unit reference volume on $\mathfrak{M}$ is assumed:

$$\psi = \psi(\boldsymbol{F}, \boldsymbol{D}, \nabla\boldsymbol{D}, \boldsymbol{G}) = \psi(F^a_A, D^A, D^A_{|B}, G_{AB}). \tag{3.3}$$

Remark 12. Independent variables entering (3.3) are motivated by the following physical and/or mathematical arguments:

- Dependence on deformation gradient $\boldsymbol{F}$ accounts for bulk elastic strain energy stored in the material (e.g., a crystal) as its atomic bonds are stretched, compressed, or sheared. This term is essential to enable the framework to reduce to classical nonlinear hyperelasticity (e.g., [61]) when the dependence of kinematics and energy on internal state is removed.
- Dependence on internal state $\boldsymbol{D}$ generally accounts for effects of microstructure features on stored energy. For example, in crystals the stored energy might depend on dislocation content, point defects, stacking faults, or twin boundaries [20,39,62].
- Dependence on the gradient of internal state $\nabla\boldsymbol{D}$ accounts for heterogeneity of microstructure. For example, this could include non-uniform distributions of defects in crystals or surface energy effects near cracks or voids. Further motivation is obtained from continuum mechanical models of liquid crystals, wherein director vector gradients may enter the thermodynamic potentials [52,63].
- This form of the energy density is also inspired by generalized continuum theories of media with microstructure [52,53], and in particular phase field theory [40,56], whereby the internal state vector $\boldsymbol{D}$ is treated here analogously to an order parameter.
- The state vector gradient dependence should enact a regularizing effect on solutions, which may simplify (e.g., numerical) computations relative to those of sharp-interface type theories that focus on surfaces of discontinuity [64,65].
- Dependence on the metric tensor $\boldsymbol{G}$ may be mathematically necessary to enable construction of scalar energy from the other material vectors and tensors that enter ψ. Furthermore, the material volume form $d\Omega$ entering variational principle (3.1) depends on $G = \det \boldsymbol{G}$ in (2.16), so it seems logical to allow ψ to also depend on the material metric. [Implicit dependence on spatial metric g_{ab} is included later in (3.5) when dependence on a material strain measure is introduced; explicit dependence on $\boldsymbol{g}$ is omitted for simplicity.]

Later in Sections 5 and 6, a more precise physical meaning will be assigned to the internal state vector in the context of example problems. Explicit dependence of energy density on particle coordinate $\boldsymbol{X}$ is omitted; such dependence could be added for materials with heterogeneous properties without affecting the governing equations derived in what follows next. Thermodynamic forces are introduced by taking the first variation of (3.3):

$$\delta\psi = \frac{\partial\psi}{\partial F^a_A}\delta F^a_A + \frac{\partial\psi}{\partial D^A}\delta(D^A) + \frac{\partial\psi}{\partial D^A_{|B}}\delta D^A_{|B} + \frac{\partial\psi}{\partial G_{AB}}\delta G_{AB} = P^A_a \delta F^a_A + Q_A \delta(D^A) + Z^B_A \delta D^A_{|B} + S^{AB}\delta G_{AB}. \tag{3.4}$$

Imposition of spatial coordinate invariance leads to the restricted form

$$\psi = \psi[\boldsymbol{C}(\boldsymbol{F}, \boldsymbol{g}), \boldsymbol{D}, \nabla\boldsymbol{D}, \boldsymbol{G}] = \psi(C_{AB}, D^A, D^A_{|B}, G_{AB}), \tag{3.5}$$

from which the first Piola–Kirchhoff stress P^A_a and Cauchy stress σ^{ab} obey

$$P^A_a = 2g_{ab}F^b_B \frac{\partial\psi}{\partial C_{AB}}, \qquad \sigma^{ab} = jg^{ac}P^A_c F^b_A = 2jF^a_A F^b_B \frac{\partial\psi}{\partial C_{AB}} = \sigma^{ba}. \tag{3.6}$$

Symmetry of Cauchy stress is consistent with the balance of angular momentum of classical continuum physics [60].

Theorem 3. *For Finsler-geometric continuum mechanics, the Euler–Lagrange equations within a compact region $\mathfrak{M}$ and natural boundary conditions on $\partial\mathfrak{M}$ corresponding to variational principle (3.1) with energy density form (3.3) are*

$$\partial_A P_a^A + P_a^B H_{AB}^A - P_c^A H_{ba}^c (F_A^b - N_A^B \bar{\partial}_B \varphi^b) + P_a^A N_A^B C_{BC}^C + (P_a^A C_{BC}^C + \bar{\partial}_B P_a^A)\partial_A D^B = 0, \tag{3.7}$$

$$\partial_A Z_C^A + Z_C^B H_{AB}^A - Z_B^A H_{AC}^B + \bar{\partial}_B Z_C^A \partial_A D^B + Z_A^B (\bar{\partial}_C N_B^A - \bar{\partial}_C K_{BD}^A D^D + \delta_C^A C_{ED}^D D_{;B}^E) + P_a^A \bar{\partial}_B \bar{\partial}_C \varphi^a \partial_A D^B - (S^{AB} + \psi G^{AB}) \bar{\partial}_C G_{AB} = Q_C; \tag{3.8}$$

$$p_a = P_a^A N_A, \qquad z_A = Z_A^B N_B. \tag{3.9}$$

Proof. Noting that variation $\delta(\cdot)$ is performed with X fixed but D variable,

$$\delta F_A^a = \delta_A(\delta\varphi^a) + \bar{\partial}_B \bar{\partial}_C \varphi^a N_A^B \delta(D^C), \qquad \delta D_{|B}^A = [\delta(D^A)]_{|B} - (\bar{\partial}_C N_B^A - \bar{\partial}_C K_{BD}^A D^D)\delta(D^C); \tag{3.10}$$

$$\delta(d\Omega) = G^{AB} \bar{\partial}_C G_{AB} \delta(D^C) d\Omega. \tag{3.11}$$

Substituting (3.4), (3.10), and (3.11) into the left side of (3.2) gives

$$\delta \int_{\mathfrak{M}} \psi \, d\Omega = \int_{\mathfrak{M}} \{P_a^A \delta_A(\delta\varphi^a) + Z_A^B [\delta(D^A)]_{|B} + [Q_C + P_a^A N_A^B \bar{\partial}_B \bar{\partial}_C \varphi^a - Z_A^B (\bar{\partial}_C N_B^A - \bar{\partial}_C K_{BD}^A D^D) + (S^{AB} + \psi G^{AB}) \bar{\partial}_C G_{AB}] \delta(D^C)\} d\Omega. \tag{3.12}$$

Two applications of the divergence theorem (2.20) and repeated integration by parts then gives the following equivalent integral form of (3.2):

$$\begin{aligned} &- \int_{\mathfrak{M}} \{[P_{a|A}^A + (P_a^A C_{BC}^C + \bar{\partial}_B P_a^A) D_{;A}^B] \delta\varphi^a + [Q_C - Z_{C|B}^B - (Z_C^A C_{BD}^D + \bar{\partial}_B Z_C^A) D_{;A}^B - Z_A^B (\bar{\partial}_C N_B^A - \bar{\partial}_C K_{BD}^A D^D) \\ &- P_a^A (\bar{\partial}_B \bar{\partial}_C \varphi^a D_{;A}^B - N_A^B \bar{\partial}_B \bar{\partial}_C \varphi^a) + (S^{AB} + \psi G^{AB}) \bar{\partial}_C G_{AB}] \delta(D^C)\} d\Omega \\ &+ \oint_{\partial\mathfrak{M}} [P_a^A N_A \delta\varphi^a + Z_A^B N_B \delta(D^A)] \Omega = \oint_{\partial\mathfrak{M}} [p_a \delta\varphi^a + z_A \delta(D^A)] \Omega. \end{aligned} \tag{3.13}$$

Assuming this global equation must hold for admissible variations $\delta\boldsymbol{x}$ and $\delta\boldsymbol{D}$, local results from (3.13) are the Euler–Lagrange equations, i.e., force balances, (3.7) and (3.8) and the Neumann boundary conditions (3.9), where (2.46) has been used in (3.7) for determining the (total) horizontal covariant derivative of two-point tensor $\boldsymbol{P} = P_a^A dx^a \otimes \frac{\delta}{\delta X^A}$.

Eq. (3.7) is the (local) balance of linear momentum for quasi-statics. Eq. (3.8) will be referred to as the (local) balance of director momentum or micro-momentum.

Remark 13. Balance equations (3.7) and (3.8) reduce as follows when configuration spaces are (pseudo)-Riemannian ($\boldsymbol{G}$ independent of D):

$$\partial_A P_a^A + P_a^B \gamma_{AB}^A - P_c^A \gamma_{ba}^c \partial_A \varphi^b + \bar{\partial}_B P_a^A \partial_A D^B = 0, \tag{3.14}$$

$$\partial_A Z_C^A + Z_C^B \gamma_{AB}^A - Z_B^A \gamma_{AC}^B + \bar{\partial}_B Z_C^A \partial_A D^B + P_a^A \bar{\partial}_B \bar{\partial}_C \varphi^a \partial_A D^B = Q_C; \tag{3.15}$$

(pseudo)-Minkowskian ($\boldsymbol{G}$ independent of X and $\boldsymbol{g}$ independent of x):

$$\partial_A P_a^A + (P_a^A C_{BC}^C + \bar{\partial}_B P_a^A) \partial_A D^B = 0, \tag{3.16}$$

$$\partial_A Z_C^A + \bar{\partial}_B Z_C^A \partial_A D^B + Z_C^B C_{AD}^D \partial_B D^A + P_a^A \bar{\partial}_B \bar{\partial}_C \varphi^a \partial_A D^B - (S^{AB} + \psi G^{AB}) \bar{\partial}_C G_{AB} = Q_C; \tag{3.17}$$

and Cartesian (global metrics $G_{AB} = \delta_{AB}$ and $g_{ab} = \delta_{ab}$):

$$\partial_A P_a^A + \bar{\partial}_B P_a^A \partial_A D^B = 0, \tag{3.18}$$

$$\partial_A Z_C^A + \bar{\partial}_B Z_C^A \partial_A D^B + P_a^A \bar{\partial}_B \bar{\partial}_C \varphi^a \partial_A D^B = Q_C. \tag{3.19}$$

4. Discussion

Essential assumptions for enacting the Finsler-geometric theory of Sections 2 and 3 are discussed in what follows next. An alternative variational principle to that set forth in Section 3 is considered in Section 4.2, which leads to a theory that reduces to existing nonlinear micromorphic theory under certain simplifying assumptions. A summary discussion of important features of the theory follows in Section 4.3.

4.1. Further theoretical assumptions

The model framework is complete upon prescription of the following details:

- For pseudo-Finsler reference space, a metric tensor $\boldsymbol{G}$ is introduced over the domain of interest in $\mathfrak{Z}$, from which all connection coefficients are derived via differentiation using relations listed in Section 2.1. In this regard, nonlinear coefficients can be determined from the spray equation (2.10), and particular forms for horizontal and vertical connection coefficients in (2.11) and (2.12) must be prescribed, e.g., those corresponding the Chern–Rund connection or Cartan's connection. The main requirement for selection of horizontal coefficients is that $(\sqrt{G})_{|A}$ must vanish for the form of divergence theorem in (2.20) to apply; this is true for Chern–Rund and Cartan connections.
- Analogous choices must be prescribed for the current configuration space, including specification of metric tensor $\boldsymbol{g}$, from which connection coefficients are derived via equations in Section 2.2. Note that same forms of metric and connections need not be prescribed in both configurations; e.g., the reference space could be taken as Finslerian and the current configuration space Riemannian, or vice-versa.
- Regarding deformation kinematics of Section 2.3, a constitutive equation may be added for specification of transformation matrices ϑ^a_B and Θ^A_b in (2.38), but this is not essential for solution of all boundary value problems. For crystals, a convenient assumption might be the Cauchy–Born rule [66,67], whereby $\vartheta^a_A(X) = F^a_A[X, D(X)]$ in a consistent coordinate basis.
- A particular form of free energy function ψ in (3.3) physically appropriate for the material of interest must also be invoked. The particular choice of course depends on the class of material (e.g., crystalline, amorphous, etc. and associated material symmetries), its deformation mechanisms and defect content, and so forth.

Then, given prescribed boundary conditions on $\partial\mathfrak{M}$, governing equations (3.7) and (3.8) represent, in principle, six coupled nonlinear partial differential equations for six unknown fields $\varphi^a[X, D(X)]$ and $D^A(X)$.

Remark 14. If Finsler geometry rather than pseudo-Finsler geometry is presumed, then a fundamental scalar function $\mathfrak{L}$ is introduced that provides $\boldsymbol{G}$ by differentiation via (2.13) rather than direct prescription, and similarly for $\mathfrak{l}$ and $\boldsymbol{g}$ via (2.33).

A few differences from (scarce) prior literature on Finsler geometry applied to continuum mechanics are noted:

- Specifically, the definition used herein for the deformation gradient (two-point) tensor in (2.39) – a partial derivative with non-holonomic basis – differs from that in [30] and [31]—a covariant derivative. The definition used here is simpler, agrees with [14], and enables computation of (2.46).
- Certain choices or options for metric tensors, connection coefficients, and energy functions vary among the present work and these prior works [30,31]; further details are apparent upon examination of each theory but are too numerous to list here.

Remark 15. Explicit time dependence of field quantities has been omitted in the present paper which has focused, for simplicity/brevity of presentation, on an incremental, quasi-static variational model. Formulation of a complete dynamic Finsler-geometric continuum theory with dissipation poses no immediately foreseeable difficulties. For example, kinetic equations extending the Ginzburg–Landau [68] or Allen–Cahn [69,70] gradient flow formalisms for state vector evolution to the present Finsler modeling framework should be readily possible. Inertia can be incorporated via extension of the Lagrangian density to allow for macroscopic and microscopic kinetic energies, as in [53], for example.

4.2. Alternative spatial representation

As an alternative to (3.1), consider the following variational principle, where now the spatial internal state vector rather than material internal state vector is treated as a fundamental independent field variable:

$$\delta\Psi(\boldsymbol{\varphi}, \boldsymbol{d}) = \oint_{\partial\mathfrak{M}} (\langle \boldsymbol{p}, \delta\boldsymbol{x}\rangle + \langle \hat{\boldsymbol{z}}, \delta\boldsymbol{d}\rangle)\Omega\,. \tag{4.1}$$

Again, Ψ is the action integral for a closed and simply connected region of $\mathfrak{M}$ with boundary $\partial\mathfrak{M}$, and surface forces are $\boldsymbol{p} = p_a dx^a$, a mechanical load vector (force per unit reference area), and $\hat{\boldsymbol{z}} = \hat{z}_a \delta d^a$, a thermodynamic force conjugate to the spatial internal state vector. Letting ψ denote potential energy density in the absence of kinetic and thermal effects, this becomes

$$\delta \int_{\mathfrak{M}} \psi\, d\Omega = \oint_{\partial\mathfrak{M}} [p_a \delta x^a + \hat{z}_a \delta(d^a)]\Omega\,, \tag{4.2}$$

where the first variation of $\boldsymbol{d}$ is enclosed in parentheses to avoid confusion with basis vector δd^a. The following functional form of the energy density per unit reference volume on $\mathfrak{M}$ is assumed:

$$\psi = \psi(\boldsymbol{F}, \boldsymbol{d}, \nabla\boldsymbol{d}, \boldsymbol{G}, \boldsymbol{g}) = \psi(F^a_A, d^a, d^a_{|B}, G_{AB}, g_{ab}). \tag{4.3}$$

Conjugate thermodynamic forces are notionally introduced by taking the first variation of (4.3):

$$\begin{aligned}\delta\psi &= \frac{\partial\psi}{\partial F^a_A}\delta F^a_A + \frac{\partial\psi}{\partial d^A}\delta(d^A) + \frac{\partial\psi}{\partial d^a_{|B}}\delta d^a_{|B} + \frac{\partial\psi}{\partial G_{AB}}\delta G_{AB} + \frac{\partial\psi}{\partial g_{ab}}\delta g_{ab}\\ &= P^A_a\delta F^a_A + Q_a\delta(d^a) + Z^B_a\delta d^a_{|B} + S^{AB}\delta G_{AB} + s^{ab}\delta g_{ab}.\end{aligned} \tag{4.4}$$

Euler–Lagrange equations and natural boundary conditions corresponding to variational principle (4.1) with energy density form (4.3) can then be derived via a procedure completely analogous to that enacted in Section 3.

Remark 16. Under assumptions of classical deformation kinematics, i.e., macro-motion independent of $\boldsymbol{D}$ or $\boldsymbol{d}$, and imposition of Riemannian rather than Finslerian geometry (e.g., basis vectors and metric tensors independent of internal state), the present theory of Section 4.2 reduces sequentially as follows:

1. Governing equations are identical, with suitable changes in notation and a constant (in time) material structure $\boldsymbol{D}$, with the static version of those of Toupin's nonlinear micromorphic theory of solids with couple stress [54], if $\boldsymbol{D}$ represents a director triad.
2. Linearization of the representation in point 1 can result in a linear micromorphic theory of Mindlin [55], which as shown in [54], is a subclass of the former.
3. Constraining the internal state vector to deform with the elastic deformation of the material reduces the representation of point 1 to a second-gradient hyperelasticity model; i.e., $\boldsymbol{\vartheta} = \boldsymbol{F}$ in a suitable basis in (2.38) results in dependence of ψ on $\nabla\boldsymbol{F}$, since then $\nabla\boldsymbol{d} \to \nabla(\boldsymbol{\vartheta})\boldsymbol{D} = \nabla(\boldsymbol{F})\boldsymbol{D}$, with $\boldsymbol{D} =$ constant.
4. Removing dependence of energy density on internal state and its gradient, and removing contributions of internal state to work done on the boundary, reduces the representation of point 1 to classical nonlinear hyperelasticity; the identical reduction can be made to the theory in Section 3.

Remark 17. When the material representation of thermodynamics in Section 3 is used in conjunction with classical deformation kinematics and a Riemannian metric tensor, the governing equations of Finsler theory can reduce to those of a variational phase field theory [40,56].

4.3. Summary

Features of the present Finsler-geometric theory that render it distinct from Riemannian-geometric approaches are summarized as follows:

- Regarding geometry, metric tensors may depend on internal state ($\boldsymbol{D}$ or $\boldsymbol{d}$), leading to possible internal state dependence of connection coefficients and volume and area forms. Nonlinear connection coefficients are introduced that affect the non-holonomic basis vectors.
- Regarding kinematics, macroscopic motion and its gradients (e.g., the deformation gradient $\boldsymbol{F}$) may depend on internal state ($\boldsymbol{D}$ or $\boldsymbol{d}$); essentially, kinematics are enhanced by extra degrees-of-freedom.
- Regarding thermodynamics, additional terms enter the Euler–Lagrange equations resulting from the above geometric and kinematic elements, including for example those involving the trace of Cartan's tensor (C^A_{BA}) arising from application of Rund's divergence theorem (2.20).

Another potential benefit is noted: the director-gradient dependence of energy and governing equations should enable regularized numerical solutions with discretization-size independence for representation of materials demonstrating softening, e.g., fracture, similarly to phase field theory [40,68,70].

5. Application: Shear failure

The first of two types of boundary value problems is considered in the present section, involving simple shearing of a two-dimensional nonlinear elastic slab. Herein, a general free energy function is postulated, applicable for any three-dimensional deformation modes, and then specified to the present geometry and kinematics.

5.1. Geometry and kinematics

The material body is an elastic slab of length L_0 and infinite width and thickness. In two dimensions, the material manifold is specified as $\{\mathfrak{M} : X^1 \in [0, L_0], |X^2| \in \infty\}$. Regarding the third (out-of-plane) direction, plane strain conditions are imposed. The internal state vector is restricted as $\{D^A\} \to \{0, D^2, 0\}$. By construction, fields vary only with $X = X^1$ and $D = D^2$, and coordinates X^3, D^1, D^3 are superfluous. A Cartesian coordinate system suffices for $\{X\}$ so metric tensor $\boldsymbol{G}$

contains no explicit dependence on X. Consistent with these protocols, the following reductions of definitions and identities of Section 2.1 hold:

$$\{X, Y\} = \{X^1, X^2\}, \quad D = D^2; \qquad \boldsymbol{G}(D) = \begin{bmatrix} G_{11}(D) & G_{12}(D) \\ G_{12}(D) & G_{22}(D) \end{bmatrix}, \quad G = G_{11}G_{22} - G_{12}^2; \tag{5.1}$$

$$\gamma_{ABC} = \tfrac{1}{2}(\partial_A G_{BC} + \partial_B G_{AC} - \partial_C G_{AB}) = 0, \qquad \Gamma^A = \tfrac{1}{2}\gamma^A_{BC} D^B D^C = 0, \quad N^A_B = \bar{\partial}_B \Gamma^A = 0 \Rightarrow \delta_A(\cdot) = \partial_A(\cdot); \tag{5.2}$$

$$C_{111} = C_{122} = C_{212} = 0, \quad C_{222} = G'_{22}/2, \quad C_{112} = -G'_{11}/2, \quad C_{121} = C_{211} = G'_{11}/2, \quad C_{221} = G'_{12}. \tag{5.3}$$

Here, $G'_{AB} = \mathrm{d}G_{AB}/\mathrm{d}D$. The reference configuration space is locally Minkowskian. The Chern–Rund connection is chosen for the following reasons. Firstly, the horizontal covariant derivative of the metric vanishes with respect to this connection [e.g., leading to $(\sqrt{G})_{|A} = 0$], so the use of Rund's version of Stokes' theorem of (2.20) to derive Euler–Lagrange equations is valid. Secondly, vertical connection coefficients (V^A_{BC}, V^a_{bc}, Y^A_{BC}, and Y^a_{bc}) are all null by definition, which simplifies computations. Thirdly, the same connection has been advocated in prior work on Finsler-geometric mechanics [30,31]. However, physics does not necessarily preclude selection of a different connection. Invoking the Chern–Rund connection with vanishing nonlinear connection coefficients from (5.2),

$$H^A_{BC} = K^A_{BC} = \Gamma^A_{BC} = \tfrac{1}{2}G^{AD}(\delta_C G_{BD} + \delta_B G_{CD} - \delta_D G_{BC}) = 0; \qquad V^A_{BC} = Y^A_{BC} = 0. \tag{5.4}$$

For the current/deformed configuration of the slab, with deformed material manifold $\{\mathfrak{m} : x^1 \in [0, L], |x^2| \in \infty\}$, where L is the deformed length of the domain, spatial coordinates and metric are of the analogous form

$$\{x, y\} = \{x^1, x^2\}, \quad d = d^2; \qquad \boldsymbol{g}(d) = \begin{bmatrix} g_{11}(d) & g_{12}(d) \\ g_{12}(d) & g_{22}(d) \end{bmatrix}, \quad g = g_{11}g_{22} - g_{12}^2; \tag{5.5}$$

$$\gamma_{abc} = \tfrac{1}{2}(\partial_a g_{bc} + \partial_b g_{ac} - \partial_c g_{ab}) = 0, \qquad \gamma^a = \tfrac{1}{2}\gamma^a_{bc} d^b d^c = 0, \quad n^a_b = \bar{\partial}_b \gamma^a = 0 \Rightarrow \delta_a(\cdot) = \partial_a(\cdot); \tag{5.6}$$

$$C_{111} = C_{122} = C_{212} = 0, \quad C_{222} = g'_{22}/2, \quad C_{112} = -g'_{11}/2, \quad C_{121} = C_{211} = g'_{11}/2, \quad C_{221} = g'_{12}; \tag{5.7}$$

with $g'_{ab} = \mathrm{d}g_{ab}/\mathrm{d}d$. The current configuration space is also locally Minkowskian. Invoking the Chern–Rund connection with vanishing nonlinear connection coefficients from (5.6),

$$H^a_{bc} = K^a_{bc} = \Gamma^a_{bc} = \tfrac{1}{2}g^{ad}(\delta_c g_{bd} + \delta_b g_{cd} - \delta_d g_{bc}) = 0; \qquad V^a_{bc} = Y^a_{bc} = 0. \tag{5.8}$$

In summary, for the present problem, nonlinear connection coefficients (N^A_B and n^a_b) vanish identically in both configurations, as do Chern–Rund coefficients (Γ^A_{BC} and Γ^a_{bc}), features which greatly simplify calculations. Cartan's coefficients (C^A_{BC} and C^a_{bc}) do not vanish, however, unless of course the metric/geometry is Riemannian.

Motions, deformations, and director gradients defined in Section 2.3 reduce as follows under simple shear, with $\varphi = \upsilon + Y$ and a denoting respective deformation and strain in the shearing (Y) direction:

$$x = X, \quad y = \varphi(X, Y, D) = Y + \upsilon(X, D); \qquad d = \vartheta(X, D); \qquad D = D(X); \tag{5.9}$$

$$\boldsymbol{F}(X, D) = \begin{bmatrix} \partial x(X)/\partial X & \partial x(X)/\partial Y \\ \partial \varphi(X, Y, D)/\partial X & \partial \varphi(X, Y, D)/\partial Y \end{bmatrix} = \begin{bmatrix} 1 & 0 \\ \partial \upsilon(X, D)/\partial X & 1 \end{bmatrix} = \begin{bmatrix} 1 & 0 \\ a(X, D) & 1 \end{bmatrix}; \tag{5.10}$$

$$J(X, D) = \sqrt{g[d(X, D)]/G(D)}F^1_1(X, D)F^2_2(X, D) = [g(X, D)/G(D)]^{1/2}; \tag{5.11}$$

$$C_{11} = g_{11} + a^2 g_{22}, \quad C_{12} = C_{21} = a g_{22} + 2g_{12}, \quad C_{22} = g_{22}; \tag{5.12}$$

$$D^2_{|1} = \partial_1 D - N^2_1 + K^2_{12} D = \partial D/\partial X = D'. \tag{5.13}$$

The internal state variable D is physically identified with a slip discontinuity or slipped displacement. The defect associated with D could be a shear band in a metal [71], a stacking fault in a crystal lattice [20], or a mode II crack in a brittle solid [40]. A more comprehensive discussion follows later in Section 5.3 in the context of the specific material considered in problem solutions.

Introduced are a constant l with dimensions of length and a normalized order parameter $\xi \in [0, 1]$:

$$\xi = D/l, \qquad \xi' = D'/l. \tag{5.14}$$

Constant l is identified as the value of shear slip-displacement D at which the slab supports no shear stress. Letting k denote a constant depending on the material, a more specific form of the Minkowski metric in (5.1) is now invoked:

$$\boldsymbol{G}(D) = \begin{bmatrix} \sqrt{G(D)} & 0 \\ 0 & \sqrt{G(D)} \end{bmatrix}; \qquad G(\xi) = \exp(2k\xi) \Rightarrow G'/(2G) = G'_{11}/G_{11} = G'_{22}/G_{22} = k/l. \tag{5.15}$$

This can be viewed as a Weyl transformation or Weyl rescaling [45] of the Cartesian metric δ_{AB}. Also used later is the second component of the trace of Cartan's tensor of (5.3):

$$C^A_{2A} = G^{AB}C_{2AB} = \tfrac{1}{2}(G^{11}G'_{11} + G^{22}G'_{22} + 4G^{12}G'_{12}) = k/l. \tag{5.16}$$

The length of a referential line element in (2.15) and the corresponding volume form in (2.16) become

$$|\mathrm{d}\boldsymbol{X}|^2 = \exp(kD/l)(\mathrm{d}X\cdot\mathrm{d}X + \mathrm{d}Y\cdot\mathrm{d}Y), \qquad d\Omega = \sqrt{G}\mathrm{d}X\wedge\mathrm{d}Y = \exp(kD/l)\mathrm{d}X\wedge\mathrm{d}Y. \tag{5.17}$$

For $\xi > 0$, expansion occurs when $k > 0$ and contraction when $k < 0$. Physical justification for this choice of metric is as follows:

- Shear fractures may result in dilatation as rough crack faces slide over one another [72,73].
- Nucleated dislocations and partial dislocations associated with shear bands or stacking faults may result in local dilatation due to nonlinear elastic and core effects [74].
- Pores may nucleate and open within shear bands in ductile solids [75].
- Shear instability can often be associated with local disordering of the lattice and amorphization, with commensurate volumetric expansion [76].

Because $\boldsymbol{G}$ is not homogeneous of degree zero in D, the reference configuration space is not strictly of Finsler character, but is a generalized pseudo-Finsler space [16], and because $\boldsymbol{G}$ does not depend explicitly on X, this space may be further categorized as pseudo-Minkowskian. Kinematics are still Finslerian since macro-motion φ can potentially depend explicitly on both D and X rather than just X.

For simplicity, the spatial and referential state variables are chosen to coincide in (5.9):

$$d(X,D) = \vartheta(X,D) = D(X) = l\xi(X). \tag{5.18}$$

Alternative transformations ϑ are mathematically possible but presently not physically justified for this example problem. An analogous form of the spatial metric is chosen for the same reasons:

$$\boldsymbol{g}(d) = \begin{bmatrix} \sqrt{g(d)} & 0 \\ 0 & \sqrt{g(d)} \end{bmatrix}; \qquad g(\xi) = \exp(2k\xi) \Rightarrow g'/(2g) = g'_{11}/g_{11} = g'_{22}/g_{22} = k/l. \tag{5.19}$$

This is a Weyl transformation or Weyl rescaling of the Cartesian metric δ_{ab}. With these choices of metrics, (5.11) and (5.12) reduce to, and give with $C_3^3 = 1$ for plane strain,

$$J = 1; \qquad C_{11} = (1+a^2)\sqrt{G}, \quad C_{12} = C_{21} = a\sqrt{G}, \quad C_{22} = \sqrt{G}; \qquad C_A^A = G^{AB}C_{AB} = a^2 + 3. \tag{5.20}$$

5.2. Energy, thermodynamic forces, and balance laws

For a hyperelastic solid with strain energy function W depending on deformation tensor $\boldsymbol{C}$, the following general form of total free energy density (3.5) is assumed:

$$\psi(C_{AB}, D^A, D^A_{|B}, G_{AB}) = W(C^A_B, D^A) + f(D^A, D^A_{|B}), \tag{5.21}$$

where function f accounts for surface energy of the microstructure, here specifically energy of crack surfaces, slip bands, and other structural defects in their vicinity. Specifically, let μ and λ denote the usual isotropic elastic constants, and let Υ be a surface energy per unit reference area (a constant material property). Then invoke

$$W = (1-|\boldsymbol{D}|/l^2)^2 W_0(C^A_B) = [1-(D^AD^B\delta_{AB}/l^2)]^2[\tfrac{1}{2}\mu(C^A_A - 3) - \mu\ln J + \tfrac{1}{2}\lambda(\ln J)^2], \tag{5.22}$$

$$f = (\Upsilon/l)(D^AD^B\delta_{AB}/l^2 + D^A_{|B}\delta_{AC}\delta^{BD}D^C_{|D}). \tag{5.23}$$

Conceivably, any form of elastic potential W and surface energy potential f could be chosen. The rationale for particular choices in (5.22) and (5.23) is as follows:

- The prefactor of $(1-|\boldsymbol{D}|/l^2)^2$ on W_0 accounts for the degradation of the total strain energy commensurate with a loss of elastic stiffness as shear failure progresses.
- Hyperelastic potential W_0 corresponds to compressible neo-Hookean elasticity [77] which has been used elsewhere to describe the elastic response of many metals and nonmetals whose behavior is isotropic or nearly so [78,79]. This particular potential demonstrates physically realistic behavior of increasing tangent bulk and shear stiffness with increasing pressure, and it is intrinsically stable [80].
- The quadratic degradation of elastic energy in conjunction with the quadratic form used for f agrees with regularized variational models of fracture, which may demonstrate gamma-type convergence to sharp-interface solutions of Griffith fracture mechanics [81,82].
- If a Riemannian rather than Finsler metric is invoked, this form of energy density coincides with that of prior phase field theory [40], to which solutions can later be compared.

Using derivations from Section 5.1, the following forms of (5.21) and (5.23) apply for the present example, i.e., the shear boundary value problem:

$$\psi = \psi(\partial\varphi/\partial X, D, \partial D/\partial X) = \psi(\partial\upsilon/\partial X, D, \partial D/\partial X) = W(a,D) + f(D, \partial D/\partial X). \tag{5.24}$$

Written in terms of shear strain and normalized order parameter, this becomes

$$\psi = \psi(a, \xi, \xi') = W(a, \xi) + f(\xi, \xi'). \tag{5.25}$$

Adding f to the elastic strain energy W reduced under simple shear conditions in (5.20) leads to

$$\psi = \tfrac{1}{2}\mu(1-\xi)^2 a^2 + \Upsilon\xi^2/l + \Upsilon l(\xi')^2. \tag{5.26}$$

The first term on the right side of (5.26) accounts for elastic strain energy degraded by damage associated with $\xi \in [0, 1]$, and the other two terms combine to account for surface energy associated with the particular class of shear defect (shear band, stacking fault, mode II crack, etc.) under consideration. This energy function contains no explicit dependence on $G_{AB}(D)$.

A full stress tensor $\boldsymbol{P}$ associated with the general form of W in (5.22) is

$$P_a^A = \frac{\partial\psi}{\partial F_A^a} = \frac{\partial W}{\partial F_A^a} = (1-\xi)^2[\mu F_B^b g_{ab} G^{AB} + (\lambda \ln J - \mu)F^{-1}{}_a^A] = (1-\xi)^2[\mu F_B^b \delta_{ab}\delta^{AB} + (\lambda \ln J - \mu)F^{-1}{}_a^A]. \tag{5.27}$$

With $F_1^2 = -(F^{-1})_2^1 = a$ and $J = 1$ in (5.27), this yields the only nonzero stress components, specifically shear stresses,

$$P = P_2^1 = P_1^2 = \mu(1-\xi)^2 a. \tag{5.28}$$

The balance of angular momentum in (3.6) is satisfied since, for the present problem,

$$\sigma^{ab} = \sigma^{ba} \Leftrightarrow P_1^2 = P_2^1 - aP_1^1 = P_2^1. \tag{5.29}$$

The other relevant, i.e., possibly nonzero, thermodynamic forces of Section 3 are then obtained by direct calculation as

$$Q = Q_2 = \frac{\partial\psi}{\partial D} = \frac{1}{l}\frac{\partial\psi}{\partial\xi} = -\frac{\mu}{l}(1-\xi)a^2 + 2\frac{\Upsilon}{l^2}\xi = -\frac{Pa}{l(1-\xi)} + 2\frac{\Upsilon}{l^2}\xi; \tag{5.30}$$

$$Z = Z_2^1 = \frac{\partial\psi}{\partial D'} = \frac{1}{l}\frac{\partial f}{\partial\xi'} = 2\Upsilon\xi'. \tag{5.31}$$

Substituting from (5.16), linear momentum balance (3.7) or (3.16) becomes

$$\frac{\partial P(X,D)}{\partial X} + \frac{\partial P(X,D)}{\partial D}\frac{\partial D}{\partial X} + P\frac{G'(D)}{2G(D)}\frac{\partial D}{\partial X} = \frac{\mathrm{d}P}{\mathrm{d}X} + P\frac{G'}{2G}\frac{\mathrm{d}D}{\mathrm{d}X} = 0. \tag{5.32}$$

Similarly, micro-momentum balance (3.8) or (3.17) becomes

$$\frac{\partial Z(X,D)}{\partial X} + \left[\frac{\partial Z(X,D)}{\partial D} + Z\frac{G'(D)}{2G(D)} + P\frac{\partial^2\upsilon(X,D)}{\partial D^2}\right]\frac{\partial D}{\partial X} - \frac{G'(D)}{G(D)}\psi(X,D) = Q(X,D). \tag{5.33}$$

Using (5.15), (5.30), and (5.31), these equilibrium equations become, respectively,

$$\frac{\mathrm{d}P}{\mathrm{d}X} = -kP\frac{\mathrm{d}\xi}{\mathrm{d}X}; \qquad P\left[\frac{a}{1-\xi} + \frac{\partial^2\upsilon}{\partial\xi^2}\xi'\right] + 2\Upsilon l\xi'' - 2\frac{\Upsilon}{l}\xi = 2k[\psi - \Upsilon l(\xi')^2]. \tag{5.34}$$

Relations (5.34) are two coupled nonlinear differential equations wherein field variables P, a, ξ, $\upsilon = \varphi - Y$, and ψ depend ultimately on independent position variable X.

5.3. Material properties

In this work, magnesium (Mg) is chosen as a representative material for which calculations are conducted. In its ambient solid state, magnesium is a low density crystalline metal of moderate ductility [83]. Its crystal structure is hexagonal. Elastic anisotropy is very low [84], and bulk and shear moduli increase with pressure, justifying the use of a compressible neo-Hookean elastic potential W_0 such as (5.22). Representative material parameters with supporting references are listed in Table 1; if no reference is listed, the value is obtained from the source given in the row above. All parameters are self-explanatory except for regularization length l and Weyl dilatation k. Regularization length l is chosen in a physically appropriate manner as the cohesive fracture process zone size over which the stress at a crack tip degrades [85,86]:

$$l = 4\mu\Upsilon/[(1-\nu)\pi\tau^2] = 16\pi\Upsilon c^2/[(1-\nu)\mu a^2]. \tag{5.35}$$

Here, ν is Poisson's ratio, $\tau = \frac{\mu}{2\pi}\frac{a}{c} \approx \frac{\mu}{10}$ is theoretical shear strength, and c and a are the hexagonal lattice parameters. From (5.17), the ratio of volume after dilatation/contraction in a fully degraded region with null shear modulus [$\xi = 1 \rightarrow \mu(1-\xi)^2 = 0$] is $\exp(k)$. For magnesium polycrystals deformed in uniaxial compression experiments, an overall volume increase of ≈2% was reported in conjunction with shear fracture modes [87]. For pure magnesium, a theoretical treatment relating shear instability to amorphization in the failure zone suggests a volume increase of ≈12% [76]. Therefore, the investigated range of $0 \le k \le \ln(1.2)$ seems physically reasonable for this material, with the lower limit corresponding to null dilatation from defects.

Table 1
Physical properties of magnesium.

Property [Units]	Value	Description	Reference
μ [GPa]	19	Shear modulus	[56]
λ [GPa]	24	Lamé modulus	
K [GPa]	37	Bulk modulus	
ν	0.28	Poisson's ratio	
c, a [nm]	0.52, 0.32	Lattice parameters	
μ'	1.3	Pressure derivative of shear modulus	[88]
K'	3.9	Pressure derivative of bulk modulus	
Υ [J/m^2]	0.69	Surface energy	[83]
exp(k)	1.0–1.2	Dilatation	[76,87]
Ξ [eV]	0.79	Vacancy formation energy	[89]

5.4. Problem solutions

Considered now is a referential configuration space that is pseudo-Finslerian when $k \neq 0$ in (5.15); when $k = 0$, the geometry is Riemannian. Even though the metric tensors are pseudo-Minkowskian, deformation kinematics are of Finsler nature since motion $\varphi = \upsilon(X, D)$ may depend on internal state. Balance laws (5.34) apply; the first results in

$$\mathrm{d}P/P = -k\mathrm{d}\xi \Rightarrow P = P_0 \exp(-k\xi), \tag{5.36}$$

where P_0 is a constant shear stress corresponding to $k = 0$ and/or $\xi = 0$. Solution of the second balance equation in (5.34) requires more precise boundary conditions. Two problems corresponding to two different sets of boundary conditions are addressed in turn: (i) localized damage corresponding to a globally stress-free deformed state, i.e., complete shear failure of the slab along a plane $X =$ constant, and (ii) accumulating homogeneous damage of the slab over $X \in [0, L_0]$, i.e., microscopic shear fractures or slip bands $D = D^2 = l\xi$ evenly distributed along the finite length of the slab.

5.4.1. Stress-free state

For a stress-free state, $P = P_0 = 0 \forall X \in [0, L_0]$. Boundary conditions on $\xi(X)$ are prescribed as

$$\xi(0) = D(0)/l = 1, \qquad \xi(L_0) = 0. \tag{5.37}$$

Boundary conditions on motion φ along the plane $Y = 0$ are prescribed as

$$\varphi(0, D) = \upsilon(0, l) = \upsilon_0, \qquad \varphi(L_0, D) = \upsilon(L_0, 0) = \upsilon_L, \tag{5.38}$$

where υ_0 and υ_L are constants. The second of governing equations (5.34), with reduced form of energy density in (5.26), becomes the nonlinear second-order ordinary differential equation

$$\xi'' - \xi/l^2 + k[(\xi')^2 - \psi/(\Upsilon l)] = 0 \Rightarrow \xi'' = (\xi/l^2)(1 + k\xi). \tag{5.39}$$

Defining $\zeta = \xi'$ such that $\xi'' = \zeta \cdot \mathrm{d}\zeta/\mathrm{d}\xi$, this can be transformed into the non-homogeneous first order differential equation and corresponding general solution

$$\zeta\,\mathrm{d}\zeta = (\xi/l^2)(1 + k\xi)\mathrm{d}\xi \Rightarrow \zeta = \pm(\xi/l)\sqrt{1 + 2k\xi^2/3 + c_0/\xi^2}, \tag{5.40}$$

with c_0 an integration constant. The latter can be rewritten and then integrated to give

$$\mathrm{d}\xi = -(\xi/l)\sqrt{1 + 2k\xi^2/3}\,\mathrm{d}X \Rightarrow X(\xi) = \int_1^{\xi} \frac{-l\mathrm{d}\beta}{\beta\sqrt{1 + 2k\beta^2/3}}. \tag{5.41}$$

The null stress condition requires

$$a(X, D) = \partial\upsilon(X, D)/\partial X = 0 \forall \xi(X) \neq 1. \tag{5.42}$$

A general solution for displacement and a particular solution satisfying boundary conditions along $Y = 0$ are thus, respectively,

$$\varphi(X, D) = \upsilon(X, D) = \bar{\upsilon}(D); \qquad \bar{\upsilon} = \upsilon_0 = \upsilon_L = \text{constant}. \tag{5.43}$$

In other words, the latter particular stress-free solution requires $\upsilon_0 = \upsilon_L$, physically corresponding to rigid body displacement by an arbitrary constant in the direction of shear. The spatial representation of the slab is considered fully failed and detached from its reference endpoint $X = 0$. Total energy per unit cross-sectional area of the slab is the line integral

$$\Psi(\xi) = \Psi_F = \int_0^{L_0} \Upsilon[(\xi')^2 l + \xi^2/l]\mathrm{d}X. \tag{5.44}$$

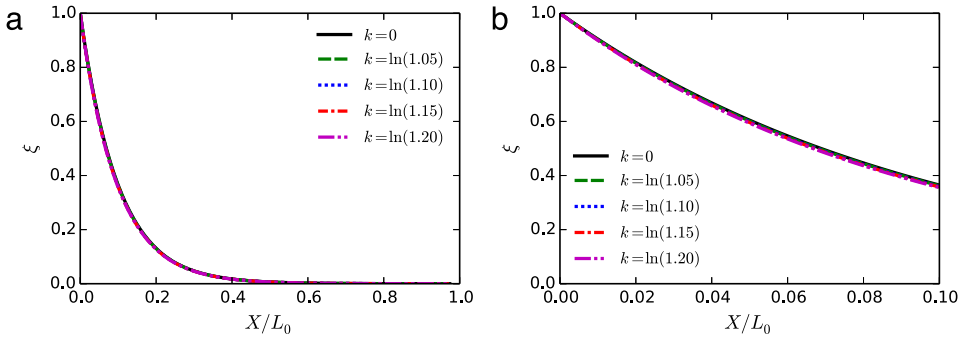

Fig. 1. Shear problem, stress-free solutions, $l/L_0 = 0.1$ (a) ξ: $0 \le X \le L_0$ (b) ξ: $0 \le X \le 0.1L_0$.

Table 2
Stress-free solutions for $l/L_0 = 0.1$ and $l/L_0 = 10^{-3}$: normalized total energy; and critical displacement and shear stress for energetically favorable transition from homogeneous to localized solutions.

Weyl scaling factor	Ψ_F/Υ $l = 0.1L_0$	Ψ_F/Υ $l = 10^{-3}L_0$	υ_C $l = 10^{-3}L_0$	$P_C/\mu \cdot 100$ $l = 10^{-3}L_0$
$k = 0$	1.00911	1.00000	0.0086	0.858
$k = \ln(1.05)$	1.00915	1.00004	0.0086	0.858
$k = \ln(1.10)$	1.00927	1.00015	0.0086	0.858
$k = \ln(1.15)$	1.00946	1.00033	0.0086	0.859
$k = \ln(1.20)$	1.00969	1.00056	0.0086	0.859

When $k = 0$, an analytical solution can be obtained in exact form. In this case, the second of governing equations (5.34) becomes

$$\xi'' - \xi/l^2 = 0 \Rightarrow \xi(X) = c_1 \exp(X/l) + c_2 \exp(-X/l). \tag{5.45}$$

Integration constants c_1, c_2 are determined by boundary conditions (5.37), leading to

$$\xi(X) = \frac{\exp(-X/l)}{1 - \exp(2L_0/l)}[\exp(2X/l) - \exp(2L_0/l)]. \tag{5.46}$$

Remark 18. Equations in (5.45) are results identical to those of a phase field theory of shear failure [40].

Shown in Fig. 1 are profiles of ξ computed via (5.41), with a domain size of $L_0 = 10l$ and the physically valid range of Weyl scaling factor k given in Table 1. Regardless of k, the value of ξ drops off rapidly from its maximum at $X = 0$ with increasing X. Increasing k results in a small decrease in ξ for $X < L_0$, and an increase in $|\xi'|$, i.e., a sharper fracture profile. The total energy per unit cross-sectional area of the bar computed via (5.44) is shown in column 2 of Table 2, normalized by intrinsic surface energy Υ. This energy Ψ_F increases very slightly with increasing k. A value of $\Psi_F = \Upsilon$ corresponds to Griffith's theory of mode II fracture, recalling that material property Υ is surface energy. Results in Table 2 therefore verify that the Finsler model correctly predicts the fracture surface energy in a domain with a localized, fully failed zone, regardless of the choice of $k \in [0, \ln(1.2)]$. Total energy does not vary significantly with increases in L_0 at fixed l, since the order parameter and its gradient tend towards null values for $X \gg l$. As shown in Table 2, as the ratio l/L_0 decreases, convergence towards the exact Griffith result is evident.

5.4.2. Homogeneous damage

For homogeneous damage, $\xi'(X) = 0 \forall X \in [0, L_0] \Rightarrow \xi(0) = \xi(L_0) = \xi_H$. Boundary conditions on displacement $\upsilon = \varphi - Y$ are prescribed as

$$\upsilon(0, D) = \upsilon_0 = D = l\xi_H, \qquad \upsilon(L_0, D) = \upsilon_L = a_H L_0 + l\xi_H. \tag{5.47}$$

Here, υ_L is the prescribed displacement of the deformed slab at $x = L$, with a_H and ξ_H constants. Specifically, a_H is a homogeneous shear strain and the product $l\xi_H$ represents rigid body displacement in the direction of shear fracture. Eqs. (5.34) and (5.36) give

$$P = P_0 \exp(-k\xi_H) = \mu(1 - \xi_H)^2 a_H = \text{constant}, \qquad \mu a_H^2(1 - \xi_H) - 2(\Upsilon/l)\xi_H = 2k\psi(a_H, \xi_H). \tag{5.48}$$

Given υ_L, (5.47) and (5.48) can be solved simultaneously for ξ_H, P_0, and a_H. Kinematics are consistent with a separable decomposition of the motion function:

$$\varphi[X, \xi(D), Y] = \upsilon(X, D) + Y = \chi(X) + Y + l\xi(D), \qquad a = F_1^2 = \mathrm{d}\chi/\mathrm{d}X = \chi', \tag{5.49}$$

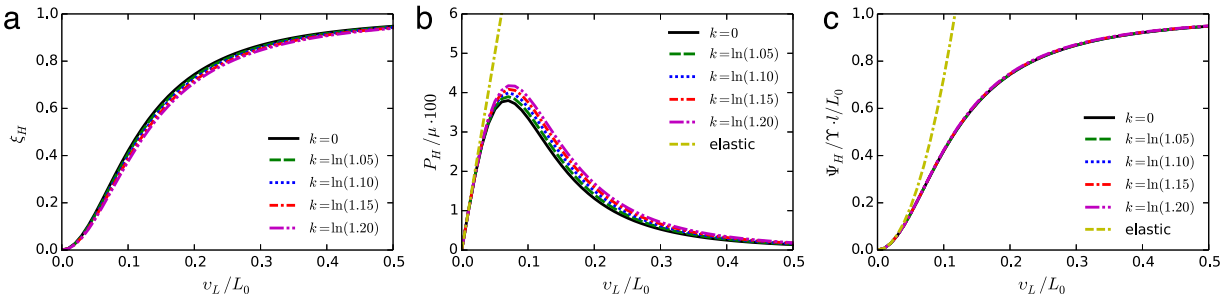

Fig. 2. Shear deformation, homogeneous solutions, $l/L_0 = 10^{-3}$ (a) order parameter $\xi = D/l$ (b) normalized shear stress (c) normalized total energy.

where for homogeneous internal structure and strain fields,

$$\varphi(X, \xi_H, Y) = a_H X + Y + l\xi_H, \qquad \chi = a_H X, \qquad F_1^2 = a_H. \tag{5.50}$$

The total energy per unit cross-section of the elastic slab with homogeneous internal structure is

$$\Psi(v_L, \xi_H) = \Psi_H = \int_0^{L_0} [\mu(1-\xi_H)^2 a_H^2/2 + \Upsilon\xi_H^2/l]\mathrm{d}X = [\mu(1-\xi_H)^2 a_H^2/2 + \Upsilon\xi_H^2/l]L_0. \tag{5.51}$$

Remark 19. Letting $\varphi(X, Y, D) \to \varphi(X, Y) = \chi(X)+Y$ and modifying (5.47) to classical (rather than Finsler-type) boundary conditions $v_0 = 0$, $v_L = a_H L_0$ recovers a description identical to phase field theory [40].

Shown in Fig. 2 are $\xi = \xi_H$, $P = P_H$, and $\Psi = \Psi_H$ versus applied shear displacement, computed via (5.48) and (5.51). These results are obtained for a domain size of $L_0 = 10^3 l$ and physical parameters for fracture of Mg along its basal planes [83] from Table 1. For fixed k, ξ increases monotonically with increasing shear displacement [Fig. 2(a)], shear stress P increases to a maximum and then decreases [Fig. 2(b)], and energy Ψ increases monotonically [Fig. 2(c)]. As k increases, ξ tends to decrease for $0 < v_L/L_0 < 0.5$, while P and Ψ tend to increase. Peak shear stress and applied displacement at which peak stress is attained both increase with increasing k, implying an increase in shear strength and stability of the material commensurate with microscopic dilatation represented mathematically by $k > 0$. Increases in stress and energy correlate with a decrease in order parameter since both P and strain energy density W are affected by a multiplication factor of $(1-\xi)^2$: see (5.22) and (5.28). The contribution of the $l\xi_H$ term in (5.50) is negligible for $l/L_0 \ll 1$, so the present Finsler solution with $k = 0$ and phase field theory [40] provide nearly identical results when microscopic dilatation is omitted. Also shown for comparison in Fig. 2(b) and (c) are shear stress and strain energy predicted by the purely elastic solution corresponding to $\xi = 0 \forall X \in [0, L_0]$. Realistically, stress and energy for the elastic solution that omits fracture far exceed those for the Finsler solution that address loss of stiffness and strength. The purely elastic solution can be obtained by taking $\Upsilon/l \to \infty$ in the Finsler theory, such that $\xi_H \to 0$ is the trivial homogeneous hyperelastic solution. Setting the regularization length to zero simultaneously eliminates the Finsler contribution to macro-motion in (5.50) and penalizes finite values of ξ_H in the energy functional (5.51) such that the only homogeneous solution is the trivial one with $\xi_H = 0$.

Consider now the relative stability of homogeneous versus localized stress-free solutions, the latter derived in Section 5.4.1. Transition from a homogeneous deformation/damage state to a state with localized fracture becomes energetically favorable at an applied deformation $v_L \geq v_C$, the applied displacement when Ψ_H of (5.51) equals or exceeds Ψ_F of (5.44), i.e., when the homogeneous solution becomes unstable. Values of v_C and corresponding shear stress P_C at the onset of such instability are listed in the rightmost two columns of Table 2, for $l/L_0 = 10^{-3}$. Predicted shear strain at instability is on the order of 1% and stress on the order of 1% of the elastic shear modulus.

5.4.3. Discussion

Solutions depicted in Fig. 1 and Table 2 demonstrate close agreement of shear failure or mode II fracture energies among the present theory, phase field theory, and Griffith's theory. Physically, the pseudo-Finsler theory predicts that dilatation is associated with an increase in slip strength or crack sliding resistance as well as failure energy, as demonstrated by solutions in Fig. 2. Such predictions agree with physical observations [72,90]: in an intensely sheared zone, effects of microscopic friction or locking of asperities increase when the material dilates in such a zone. For values of k appropriate for the material presently under consideration, the dilatation may be the result of locally heterogeneous (i.e., imperfect) microscopic fractures in the damaged zone (as opposed to perfect cleavage) [87] or expansion due to lattice disordering in a structurally unstable region of intense shear [76]. In particular, toughening associated with dilatation commensurate with intense microcracking has been noted in fracture of ice [90], with characteristics similar to those for metals with hexagonal symmetry [73], e.g., Mg. Such toughening cannot be predicted by the Riemannian reduction of the theory corresponding to $k = 0$, which does not include physics of dilatation. In other materials or loading regimes, dilatation could also arise from nonlinear elastic effects associated with defect cores (e.g., dislocation cores, point defects, and stacking faults) [74], and/or thermal expansion due to temperature rise in adiabatic shear [71]. It should be noted however, that the present variational model does not explicitly monitor time dependent dissipated energy associated with sliding friction or dislocation glide.

6. Application: Spherical expansion and cavitation

The second of two types of considered boundary value problems involves radial expansion of a spherical nonlinear elastic body. Cavitation, i.e., void or vacancy formation and growth, may occur uniformly throughout the domain or localized at or very near to the center of the sphere, depending on particular boundary conditions imposed in what follows. A general free energy function is postulated as in Section 5 and then specialized to the current geometry, but here curvilinear – specifically, spherical – coordinates are needed. This complicates the present analysis relative to that considered in Section 5 that was tractable via Cartesian frames. The metric tensors necessarily depend explicitly on position and may also depend on the internal state; when the latter applies, a completely pseudo-Finslerian configuration space results.

6.1. Geometry and kinematics

The material body is an elastic sphere of radius R_0. The referential material manifold is specified as $\{\mathfrak{M} : R = X^1 \in [0, R_0], \Theta = X^2 \in [0, \pi], \Phi = X^3 \in (-\pi, \pi]\}$. By construction, spherical symmetry conditions are imposed so that solution field variables do not depend on angular coordinates Θ, Φ. The internal state vector is restricted to have a radial component only: $\{D^A\} \to \{D^1, 0, 0\}$ with $D^1 = D^R$. Metric tensor $\boldsymbol{G}$ necessarily depends on X and possibly depends on D. Consistent with these protocols, definitions and identities of Section 2.1 result in

$$\{R, \Theta, \Phi\} = \{X^1, X^2, X^3\}, \qquad \{D^1, D^2, D^3\} = \{D, 0, 0\}. \tag{6.1}$$

Denoting by $\bar{\boldsymbol{G}} = \bar{\boldsymbol{G}}(X)$ the usual metric tensor of Euclidean space in spherical coordinates [23,61] and $B = B(D)$ a differentiable scalar function of the internal state, the following multiplicatively separable form of the metric tensor $\boldsymbol{G}(X, D)$ is assumed:

$$\begin{aligned} &\boldsymbol{G}(X, D) = \bar{\boldsymbol{G}}(X)B(D) = \begin{bmatrix} \bar{G}_{11} & 0 & 0 \\ 0 & \bar{G}_{22}(X) & 0 \\ 0 & 0 & \bar{G}_{33}(X) \end{bmatrix} B(D) = \begin{bmatrix} 1 & 0 & 0 \\ 0 & R^2 & 0 \\ 0 & 0 & R^2 \sin^2\Theta \end{bmatrix} B(D), \\ &G = B^3\bar{G} = B^3R^4 \sin^2\Theta. \end{aligned} \tag{6.2}$$

Let $\bar{\gamma}^A_{BC}$ denote Christoffel symbols of the second kind derived from $\bar{\boldsymbol{G}}$, and let γ^A_{BC} denote those derived from $\boldsymbol{G}$. From (2.7) and (6.2), these are equivalent:

$$\gamma^A_{BC} = G^{AD}\gamma_{BCD} = (B^{-1}\bar{G}^{AD})(B\bar{\gamma}_{BCD}) = \bar{\gamma}^A_{BC}. \tag{6.3}$$

Nonzero Christoffel symbols resulting from (6.2) are thus, with indices $(1, 2, 3) \leftrightarrow (R, \Theta, \Phi)$ [23,61],

$$\gamma^\Theta_{R\Theta} = \gamma^\Phi_{R\Phi} = 1/R, \quad \gamma^R_{\Theta\Theta} = -R, \quad \gamma^\Phi_{\Theta\Phi} = \cot\Theta, \quad \gamma^R_{\Phi\Phi} = -R\sin^2\Theta, \quad \gamma^\Theta_{\Phi\Phi} = -\sin\Theta\cos\Theta. \tag{6.4}$$

Since the only non-vanishing component of $\boldsymbol{D}$ is radial and since $\gamma^A_{RR} = 0$, the spray and nonlinear connection coefficients derived from it vanish identically for this problem:

$$G^A = \tfrac{1}{2}\gamma^A_{BC}D^BD^C = \tfrac{1}{2}\gamma^A_{RR}D\cdot D = 0, \qquad N^A_B = G^A_B = \bar{\partial}_B G^A = 0. \tag{6.5}$$

Denoting $B' = \partial B/\partial D^1 = \mathrm{d}B/\mathrm{d}D$, nonzero components of Cartan's tensor in (2.8) are

$$C_{111} = \tfrac{1}{2}B', \quad C_{122} = C_{212} = \tfrac{1}{2}B'R^2, \quad C_{133} = C_{313} = \tfrac{1}{2}B'R^2\sin^2\Theta, \quad C_{221} = -\tfrac{1}{2}B'R^2, \quad C_{331} = -\tfrac{1}{2}B'R^2\sin^2\Theta. \tag{6.6}$$

The trace of Cartan's tensor in the radial direction will be used later:

$$C^A_{RA} = C^1_{11} + C^2_{12} + C^3_{13} = 3B'/(2B). \tag{6.7}$$

The reference configuration space is generalized (pseudo)-Finslerian. The Chern–Rund connection is now used for the same reasons outlined following (5.3) in Section 5.1. Invoking this connection with vanishing nonlinear connection coefficients from (6.5), horizontal coefficients are equal to Levi-Civita coefficients derived from $\bar{G}_{AB}$, while vertical coefficients vanish by definition of the Chern–Rund connection:

$$H^A_{BC} = K^A_{BC} = \Gamma^A_{BC} = \gamma^A_{BC}; \qquad V^A_{BC} = Y^A_{BC} = 0. \tag{6.8}$$

Following the same general reasoning as in Section 5.1, the analogous geometric description is assumed for the current configuration space. The spatial configuration manifold is specified as $\{\mathfrak{m} : r = x^1 \in [0, r_0], \theta = X^2 \in [0, \pi], \phi = x^3 \in (-\pi, \pi]\}$. Metric tensor $\boldsymbol{g}$ necessarily depends on x in spherical coordinates, and by construction it may depend on the internal state vector, whose spatial representation $\boldsymbol{d}$ is presumed radial. Definitions and identities of Section 2.2 result in

$$\{r, \theta, \phi\} = \{x^1, x^2, x^3\}, \qquad \{d^1, d^2, d^3\} = \{d, 0, 0\}. \tag{6.9}$$

Denoting by $\bar{\boldsymbol{g}} = \bar{\boldsymbol{g}}(x)$ the conventional Riemannian metric tensor of Euclidean space in spherical coordinates [23,61] and $b = b(d)$ a differentiable scalar function of the spatial internal state, the following multiplicative separable form of the metric tensor $\boldsymbol{g}(x, d)$ is invoked:

$$\boldsymbol{g}(x) = \bar{\boldsymbol{g}}(x)b(d) = \begin{bmatrix} \bar{g}_{11} & 0 & 0 \\ 0 & \bar{g}_{22}(x) & 0 \\ 0 & 0 & \bar{g}_{33}(x) \end{bmatrix} b(d) = \begin{bmatrix} 1 & 0 & 0 \\ 0 & r^2 & 0 \\ 0 & 0 & r^2 \sin^2\theta \end{bmatrix} b(d), \quad g = b^3\bar{g} = b^3 r^4 \sin^2\theta. \tag{6.10}$$

Nonzero Christoffel symbols resulting from (6.10) are, analogously to (6.4), with indices $(1, 2, 3) \leftrightarrow (r, \theta, \phi)$ [23,61],

$$\gamma^{\theta}_{r\theta} = \gamma^{\phi}_{r\phi} = 1/r, \quad \gamma^{r}_{\theta\theta} = -r, \quad \gamma^{\phi}_{\theta\phi} = \cot\theta, \quad \gamma^{r}_{\phi\phi} = -r\sin^2\theta, \quad \gamma^{\theta}_{\phi\phi} = -\sin\theta\cos\theta. \tag{6.11}$$

Because the only non-vanishing component of $\boldsymbol{d}$ is radial ($d = d^r$) and since $\gamma^a_{rr} = 0$, the spray and nonlinear connection coefficients derived from it vanish identically:

$$g^a = \tfrac{1}{2}\gamma^a_{bc} d^b d^c = \tfrac{1}{2}\gamma^a_{rr} d \cdot d = 0, \qquad n^a_b = g^a_b = \bar{\partial}_b g^a = 0. \tag{6.12}$$

Nonzero components of Cartan's tensor in (2.28) are, with $b' = \partial b/\partial d^1 = \mathrm{d}b/\mathrm{d}d$,

$$C_{111} = \tfrac{1}{2}b', \quad C_{122} = C_{212} = \tfrac{1}{2}b'r^2, \quad C_{133} = C_{313} = \tfrac{1}{2}b'r^2\sin^2\theta, \quad C_{221} = -\tfrac{1}{2}b'r^2, \quad C_{331} = -\tfrac{1}{2}b'r^2\sin^2\theta. \tag{6.13}$$

Since nonlinear connection coefficients from the spray vanish, the horizontal Chern–Rund coefficients coincide with (6.11). Analogously to (6.8), the following horizontal and vertical connection coefficients are imposed for gradients of basis vectors:

$$H^a_{bc} = K^a_{bc} = \Gamma^a_{bc} = \gamma^a_{bc}; \qquad V^a_{bc} = Y^a_{bc} = 0. \tag{6.14}$$

Motions, deformations, and director gradients defined in Section 2.3 reduce as follows under spherical expansion or contraction, with $\varphi = r$ denoting deformation in the radial (R) direction:

$$r = \varphi(R, D) = r(R, D), \quad \theta = \Theta, \quad \phi = \Phi; \quad d = \vartheta(R, D), \quad D = D(R); \tag{6.15}$$

$$\boldsymbol{F}(R, D) = \begin{bmatrix} \partial r(R, D)/\partial R & 0 & 0 \\ 0 & \partial\theta/\partial\Theta & 0 \\ 0 & 0 & \partial\phi/\partial\Phi \end{bmatrix} = \begin{bmatrix} F^r_R(R, D) & 0 & 0 \\ 0 & 1 & 0 \\ 0 & 0 & 1 \end{bmatrix}; \tag{6.16}$$

$$J(R, D) = \sqrt{g[r, \theta, d(R, D)]/G(R, \theta, D)}F^1_1(R, D)F^2_2F^3_3 = (r^2/R^2)F^r_R(R, D)\{b[d(R, D)]/B(D)\}^{3/2}; \tag{6.17}$$

$$C_{11} = b(F^r_R)^2, \quad C_{22} = br^2, \quad C_{33} = br^2\sin^2\theta, \quad C_{12} = C_{13} = C_{23} = 0; \quad \det(C^A_B) = (F^r_R)^2(r/R)^4(b/B)^3 = J^2; \tag{6.18}$$

$$D^1_{|1} = D^R_{|R} = \partial_R D - N^R_R + K^R_{RR}D = \partial D/\partial R = D'. \tag{6.19}$$

Internal state variable D is physically identified with radial microscopic opening in the material associated with spherical expansion and cavitation. The physical defect associated with D could be a pore or void in a rock or metal or, at the nanoscale, a site vacancy in a crystal lattice. The structure variable may represent a single defect or a continuous distribution of such defects. As in Section 5, constant l with dimensions of length and a normalized order parameter $\xi \in [0, 1]$ are introduced:

$$\xi = D/l, \qquad \xi' = D'/l. \tag{6.20}$$

Constant l will later be identified as the value of radial micro-displacement D at which a material point within the sphere supports no stress. Solutions derived later will demonstrate that larger values of l correlate with an increased tendency for the material to exhibit distributed porosity/vacancy increase rather than localized cavitation. Letting k denote a constant depending on the material, a more specific form of the pseudo-Finsler metric in (6.2) is henceforth invoked:

$$\boldsymbol{G}(X, D) = \bar{\boldsymbol{G}}(X)B(D) = \bar{\boldsymbol{G}}(X)\exp(2k\xi/3), \qquad B(D) = \exp[(2kD)/(3l)] = \exp(2k\xi/3); \tag{6.21}$$

$$B'/B = \bar{\partial}_1 G_{11}/G_{11} = \bar{\partial}_2 G_{22}/G_{22} = \bar{\partial}_3 G_{33}/G_{33} = 2k/(3l). \tag{6.22}$$

This can be viewed as a Weyl transformation or Weyl rescaling [45] of the spherical Euclidean metric $\bar{G}_{AB}$. The radial component of the trace of Cartan's tensor of (6.7) is

$$C^A_{RA} = 3B'/(2B) = k/l. \tag{6.23}$$

The length of a referential line element in (2.15) and the corresponding volume form in (2.16) become

$$\begin{aligned} &|\mathrm{d}\boldsymbol{X}|^2 = \exp(2k\xi/3)(\mathrm{d}R \cdot \mathrm{d}R + R^2\mathrm{d}\Theta \cdot \mathrm{d}\Theta + R^2\sin^2\Theta\mathrm{d}\Phi \cdot \mathrm{d}\Phi), \\ &d\Omega = \exp(k\xi/3)R^2\sin\Theta\mathrm{d}R \wedge \mathrm{d}\Theta \wedge \mathrm{d}\Phi. \end{aligned} \tag{6.24}$$

For $\xi > 0$, expansion occurs when $k > 0$ and contraction when $k < 0$. Physical justification for this choice of metric is

- Cavitation is obviously associated with expansion, i.e., $k > 0$. The opposite condition, $k < 0$, would apply for collapse of existing pores, e.g., which would be expected for compressive rather than tensile loading protocols.
- Under spherically symmetric tensile loading, depending on ambient temperature and crystal type, an element of crystal may demonstrate localized cavitation (i.e., a single large defect at its core) or distributed disordering and dilatation throughout its volume similar to melting [91]. The latter disordering of the lattice and amorphization are linked quantitatively with volumetric expansion in [76].

Because $\boldsymbol{G}$ is not homogeneous of degree zero in D, the reference configuration space is a generalized pseudo-Finsler space [16]. Kinematics are also Finslerian since φ can depend explicitly on both D and X rather than just X.

As was assumed in Section 5, since such an assumption is not precluded by physics, the spatial and referential state variables are chosen to simply coincide in (6.15):

$$d(X, D) = \vartheta(X, D) = D(X) = l\xi(X). \tag{6.25}$$

Different transformations ϑ are mathematically possible but additional complexity is not physically justified for this problem. An analogous form of the spatial metric is

$$\boldsymbol{g}(x, d) = \bar{\boldsymbol{g}}(x)b(d) = \bar{\boldsymbol{g}}(x)\exp(2k\xi/3), \qquad b[d(D)] = \exp[(2kd)/(3l)] = \exp[(2kD)/(3l)] = B(D). \tag{6.26}$$

This is a Weyl transformation or Weyl rescaling of the usual spherical metric $\bar{g}_{ab}$. For notational simplicity, define the radial stretch as

$$a(R, D) = F^r_R(R, D) = \partial r(R, D)/\partial R. \tag{6.27}$$

With this notation and the above coincident choices of metrics, (6.17) and (6.18) reduce to

$$J = ar^2/R^2; \qquad C^1_1 = a^2, \quad C^2_2 = C^3_3 = r^2/R^2; \qquad C^A_A = a^2 + 2r^2/R^2. \tag{6.28}$$

The principal stretches are the physical components of diagonal matrix $\sqrt{\boldsymbol{C}}$:

$$\lambda_1 = a, \qquad \lambda_2 = \lambda_3 = r/R. \tag{6.29}$$

6.2. Energy, thermodynamic forces, and balance laws

Similarly to the model considered in Section 5.2, a compressible neo-Hookean strain energy function W depending on deformation tensor $\boldsymbol{C}$ is assumed to enter ψ of (3.5):

$$\psi(C_{AB}, D^A, D^A_{|B}, G_{AB}) = W(C^A_B, D^A) + f(D^A, D^A_{|B}), \tag{6.30}$$

where W is bulk elastic energy and function f accounts for intrinsic energy of defects such as surface energies of voids or cavities and formation energy of vacancies. More specifically let

$$W = (1 - |\boldsymbol{D}|/l^2)^2 W_0(C^A_B) = [1 - (D^A D^B \delta_{AB}/l^2)]^2 W_0(C^A_B), \quad f = (\Upsilon/l)(D^A\delta_{AB}D^B/l^2 + D^A_{|B}\delta_{AC}\delta^{BD}D^C_{|D}). \tag{6.31}$$

Function W_0 is the hyperelastic energy density in the absence of defects or internal structure. For the present problem, the following compressible neo-Hookean bulk strain energy function [92] is used:

$$W_0 = c_1(j_1 - 3) + c_2(j_2 - 3) + c_3(j_3 - 1), \tag{6.32}$$

where elastic coefficients in terms of reference shear modulus μ and Poisson's ratio ν are

$$c_1 = \mu(1 - 3\nu)/(1 - 2\nu), \qquad c_2 = \mu(1 - \nu)/(1 - 2\nu), \qquad c_3 = 2\mu\nu/(1 - 2\nu), \tag{6.33}$$

and where the following invariants of $\sqrt{\boldsymbol{C}}$ are used:

$$j_1 = \lambda_1 + \lambda_2 + \lambda_3, \qquad j_2 = 1/\lambda_1 + 1/\lambda_2 + 1/\lambda_3, \qquad j_3 = J = \lambda_1\lambda_2\lambda_3. \tag{6.34}$$

Defect energy per unit reference area is again written as Υ, treated as an intrinsic material property. As noted in Section 5.2, other forms of elastic potential W and surface energy potential f could be chosen. The rationale for particular choices in (6.30)–(6.34) is as follows:

- The prefactor of $(1 - |\boldsymbol{D}|/l^2)^2$ on W_0 accounts for the degradation of the total strain energy commensurate with a loss of elastic stiffness as local failure associated with increases in porosity progresses. As the vacancy concentration tends towards saturation at a point X, $\xi(X) \to 1$, and the tangent elastic stiffness tends towards zero, as reported for solid-state amorphization or melting [76,91].
- Hyperelastic potential W_0 corresponds to compressible neo-Hookean elasticity, which reasonably describes the elastic response of many solids whose behavior is (nearly) isotropic. This particular potential is chosen because an exact closed-form solution is available for the bifurcation problem associated with localized cavitation [92] in Riemannian hyperelasticity (i.e., null internal structure variables), described in Appendix B of this paper.

- The quadratic degradation of elastic energy in conjunction with the quadratic form used for f is used in regularized variational models that may demonstrate gamma-type convergence to sharp-interface solutions [81,82]. The form for f in (6.31) is identical to that in (5.23).

A general mechanical stress tensor $\boldsymbol{P}$ associated with $W\{\lambda_\alpha[\boldsymbol{C}(\boldsymbol{F},\bar{\boldsymbol{g}},\bar{\boldsymbol{G}})],\boldsymbol{D}\}$ is

$$P_a^A = \frac{\partial\psi}{\partial F_A^a} = \frac{\partial W}{\partial F_A^a} = (1-|\boldsymbol{D}|)^2\frac{\partial W_0}{\partial\lambda_\alpha}\frac{\partial\lambda_\alpha}{\partial F_A^a} \qquad (\alpha=1,2,3). \tag{6.35}$$

Using derivations from Section 6.1, the following form of (6.30) applies henceforth:

$$\psi = \psi(\lambda_\alpha, D, \partial D/\partial R) = W(a,r,\xi) + f(\xi,\xi') = (1-\xi)^2 W_0(a,r) + f(\xi,\xi'). \tag{6.36}$$

Adding f to the elastic strain energy W reduced under spherical deformation with (6.29) now applied leads to

$$\begin{aligned}\psi(a,r,\xi,\xi') &= (1-\xi)^2 W_0(a,r) + \Upsilon\xi^2/l + \Upsilon l(\xi')^2 \\ &= (1-\xi)^2[c_1(a+2r/R-3)+c_2(1/a+2R/r-3)+c_3(ar^2/R^2-1)] + \Upsilon[\xi^2/l + l(\xi')^2].\end{aligned} \tag{6.37}$$

For the present case of spherical symmetry, the only nonzero stress components in (6.35) are then

$$P = P_1^1 = P_r^R = (1-\xi)^2\lambda_2\lambda_3\sigma_1, \qquad P_2^2 = P_\theta^\Theta = P_3^3 = P_\phi^\Phi = (1-\xi)^2\lambda_1\lambda_2\lambda_3\sigma_2 = (1-\xi)^2\lambda_1\lambda_2\lambda_3\sigma_3, \tag{6.38}$$

where principal physical Cauchy stress components are

$$\sigma_\alpha = [1/(\lambda_1\lambda_2\lambda_3)](c_1\lambda_\alpha - c_2/\lambda_\alpha) + c_3 \qquad (\alpha=1,2,3). \tag{6.39}$$

The balance of angular momentum in (3.6) is trivially satisfied since $\boldsymbol{F}$ and $\boldsymbol{g}$ are of diagonal form and all shear stresses, i.e., off-diagonal components of mechanical stress, vanish.

Specific versions of nonzero thermodynamic forces of Section 3 are then computed as follows, with stress components consistent with (6.38):

$$P = (1-\xi)^2(r^2/R^2)\sigma_1, \qquad T = (R/2r)(P_\theta^\Theta + P_\phi^\Phi) = (1-\xi)^2(ar/R)\sigma_2 = (1-\xi)^2(ar/R)\sigma_3; \tag{6.40}$$

$$Q = Q_R = \frac{\partial\psi}{\partial D} = \frac{1}{l}\frac{\partial\psi}{\partial\xi} = 2\frac{\Upsilon}{l^2}\xi - \frac{2(1-\xi)}{l}W_0; \tag{6.41}$$

$$Z = Z_R^R = \frac{\partial\psi}{\partial D^1_{|1}} = \frac{1}{l}\frac{\partial\psi}{\partial\xi'} = \frac{1}{l}\frac{\partial f}{\partial\xi'} = 2\Upsilon\xi'. \tag{6.42}$$

Radial and transverse or circumferential stresses are denoted simply by P and T, respectively.

The following scalar function will also be invoked later, where ψ is the function in (6.37):

$$\iota(a,r,\xi,\xi') = [2B/(3B')]G^{AB}\bar{\partial}_1 G_{AB}\psi(a,r,\xi,\xi') = 2\psi(a,r,\xi,\xi') = 2(1-\xi)^2 W_0(a,r) + 2\Upsilon[\xi^2/l + l(\xi')^2]. \tag{6.43}$$

Momentum balances specific to the present problem are derived as follows. Linear momentum balance (3.7) yields the three equations ($a=1,2,3=r,\theta,\phi$):

$$\partial_A P_a^A + \bar{\partial}_B P_a^A \partial_A D^B + P_a^B\gamma_{AB}^A - P_c^A\gamma_{ba}^c F_A^b + P_a^A C_{BC}^C\partial_A D^B = 0. \tag{6.44}$$

For $a=2,3$, since $P_\theta^\Theta = P_\phi^\Phi$ from (6.38), and $\theta=\Theta$, $\phi=\Phi$ from spherically symmetric deformation, these reduce to the two trivially satisfied equations

$$P_\theta^\Theta\gamma_{A\Theta}^A - P_\phi^\Phi\gamma_{\phi\theta}^\phi F_\Phi^\phi = P_\theta^\Theta\cot\Theta - P_\phi^\Phi\cot\theta = 0, \qquad P_c^A\gamma_{b\phi}^c F_A^b = 0. \tag{6.45}$$

A non-trivial linear momentum balance remains for the radial direction $a=1=r$ in (6.44):

$$\partial_R P + \frac{\partial P}{\partial D}\frac{\partial D}{\partial R} + \frac{2}{R}P - \frac{1}{r}(P_\theta^\Theta + P_\phi^\Phi) + PC_{RA}^A\frac{\partial D}{\partial R} = 0. \tag{6.46}$$

The only non-trivial component of micro-momentum balance (3.8) is for the radial direction, $C=1=R$:

$$\frac{\partial Z}{\partial R} + \frac{2}{R}Z + \left(\frac{\partial Z}{\partial D} + P\frac{\partial^2\varphi}{\partial D^2}\right)\frac{\partial D}{\partial R} + \frac{3B'}{2B}\left(Z\frac{\partial D}{\partial R} - \iota\right) = Q. \tag{6.47}$$

Substituting from (6.23) and (6.40) leads to the following reduced form of (6.46):

$$\frac{\mathrm{d}P}{\mathrm{d}R} + \frac{2}{R}(P-T) = -kP\frac{\mathrm{d}\xi}{\mathrm{d}R}. \tag{6.48}$$

Substituting from (6.23), (6.41), (6.42), and (6.43) and multiplying (6.47) by $\frac{l}{2}$ gives

$$\Upsilon l\xi'' + \frac{2\Upsilon l}{R}\xi' - \frac{\Upsilon}{l}\xi + \frac{P}{2}\frac{\partial^2 r}{\partial\xi^2}\xi' + (1-\xi)W_0 = k\left[(1-\xi)^2 W_0 + \frac{\Upsilon}{l}\xi^2\right]. \tag{6.49}$$

Relations (6.48) and (6.49) are two coupled nonlinear differential equations wherein field variables P, a, r, ξ, and W_0 depend ultimately on independent position variable R.

6.3. Material properties

As also studied in Section 5, magnesium (Mg) is chosen as a representative material for the present spherical expansion problem. As remarked already, elastic anisotropy is very low and the bulk modulus is not excessive relative to the shear modulus ($\nu < 0.5$), justifying the use of a compressible neo-Hookean elastic potential W_0. The same representative material parameters given in Table 1 and discussed in Section 5.3 are used in what follows, with a few possible exceptions since now the physics represented by the problem differs: presently the structural defects are cavities, voids and/or vacancies rather than mode II micro-cracks or slip bands considered in Section 5. In lieu of (5.35), regularization length l is varied parametrically over a fraction of domain size R_0. Unless noted otherwise, the latter is taken as representative of atomic-scale or nanoscopic phenomena such as studied in the case of expansion and/or amorphization of metallic crystals in [76,91]: $R_0 = 10$a, corresponding to a volume on the order of 10^3 unit cells. The treatment in Appendix A of the present paper, based on arguments from condensed matter physics and nonlinear elasticity, suggests a value of $\exp(k) \approx 1.16$ is physically appropriate for vacancies in Mg. Also as noted in Section 5.3, $\exp(k) \approx 1.12$ is suggested in [76]. Thus, the range of $0 \leq k \leq \ln(1.2)$ in Table 1 again appears reasonable.

6.4. Problem solutions

Considered is the general scenario wherein the referential configuration space is pseudo-Finslerian with $k \neq 0$ in (6.21); when $k = 0$, geometry becomes Riemannian. Referential and spatial metrics are generalized pseudo-Finslerian, and deformation kinematics are of Finsler character because $r = \varphi(R, D)$ can potentially depend on D as well as R. Balance laws (6.48) and (6.49) apply in full; the second can be rearranged as

$$\Upsilon l\xi'' + \frac{2\Upsilon l}{R}\xi' - \frac{\Upsilon}{l}(1 + k\xi)\xi + \frac{P}{2}\frac{\partial^2 r}{\partial \xi^2}\xi' + (1 - \xi)[1 - k(1 - \xi)]W_0 = 0. \tag{6.50}$$

Solutions require specification of boundary conditions. Two problems corresponding to two different sets of boundary conditions are addressed. The first involves localized cavitation or vacancy nucleation corresponding to a globally stress-free state, i.e., saturated vacancy density at the core of the spherical domain: $\xi \to 1$ as $R \to 0$. The second involves homogeneous damage of the deformed sphere over $R \in [0, R_0]$, i.e., microscopic voids or vacancies $D = D^R = D^1$ evenly distributed within the volume, with the additional possibility of a discrete larger void/cavity forming at the core of the sphere. In the second case, comparison with the classical hyperelasticity solutions for cavitation [92] proves instructive.

6.4.1. Stress-free state

For a stress-free state $P = T = 0 \forall R \in [0, R_0]$. Boundary conditions on order parameter $\xi(R)$ are prescribed as

$$\xi(\varepsilon_0 R_0) = D(\varepsilon_0 R_0)/l = 1 - \varepsilon_0, \qquad \xi(R_0) = 0. \tag{6.51}$$

The general solution for ξ is singular at $R = 0$; therefore, the solution space is restricted to the domain $\epsilon_0 \leq R/R_0 \leq 1$, where $\epsilon_0 \ll 1$ is a small parameter. Micro-momentum balance (6.50) becomes, with $W_0 = 0$, the following homogeneous nonlinear second-order ordinary differential equation for state variable field $\xi = \xi(R)$:

$$\xi'' + (2/R)\xi' - (1/l^2)(1 + k\xi)\xi = 0. \tag{6.52}$$

This equation has no known general analytical solution for $k \neq 0$. Therefore, solutions are obtained numerically via a second-order accurate finite difference scheme with iterative evaluation of the nonlinear $k\xi$ term. Total energy contained in the stress-free domain is the volume integral

$$\Psi(\xi) = \Psi_F = 4\pi \int_0^{R_0} \Upsilon[(\xi')^2 l + \xi^2/l]R^2 \mathrm{d}R. \tag{6.53}$$

In the Riemannian case, i.e., when $k = 0$, an analytical solution can be obtained in closed form. Noting that W_0 vanishes for a stress-free state, (6.52) becomes the homogeneous nonlinear second-order ordinary differential equation for the field $\xi = \xi(R)$ with corresponding general solution

$$\xi'' + (2/R)\xi' - \xi/l^2 = 0 \Rightarrow \xi(R) = (1/R)[d_1 \exp(R/l) + d_2 \exp(-R/l)]. \tag{6.54}$$

With particular boundary conditions (6.51), constants d_1 and d_2 can be obtained, and the corresponding complete solution for (shown here for $R_0 = 1$ unit) is

$$\xi(R) = \frac{\varepsilon_0}{R}\frac{(1 - \varepsilon_0)\exp[-(R + \varepsilon_0)/l]}{\exp[2(1 - \epsilon_0)/l] - 1}[\exp(2R/l) - \exp(2/l)]. \tag{6.55}$$

Linear momentum balance (6.48) is trivially satisfied. However, the null stress condition requires

$$a(R, D) = \partial\varphi(R, D)/\partial R = \lambda_1 = r(r, D)/R = \lambda_2 = \lambda_3 = 1 \forall \xi(R) \neq 1. \tag{6.56}$$

In other words, the stress-free domain is macroscopically elastically undeformed.

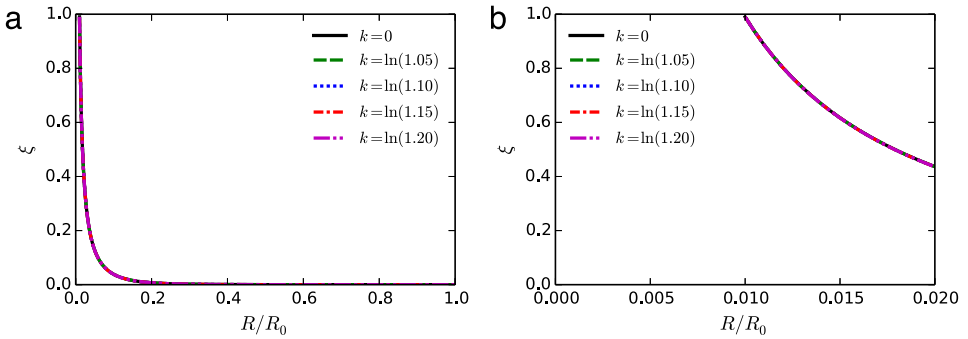

Fig. 3. Spherical domain, stress-free solutions, $l/R_0 = 0.1$ (a) ξ: $0 \le R \le L_0$ (b) ξ: $0 \le R \le 0.1L_0$.

Shown in Fig. 3 are profiles of ξ computed via the finite difference method, with $\varepsilon_0 = 0.01, R_0 = 10l$ and the range of Weyl scaling factor k considered in Table 1. Regardless of k, ξ decreases rapidly from its maximum at $R = \varepsilon_0 R_0$ with increasing R to the imposed boundary value $\xi(R_0) = 0$. Increasing k provides no apparent change in ξ for $R < R_0$ for spherical solutions in Fig. 3, in contrast to shear solutions shown in Fig. 1. The total energy calculated via (6.53) for $\exp(k) = 1.16$ is 0.88 eV. This energy Ψ_F was found to be negligibly affected by the choice of k, and its value is reasonably close to the vacancy formation energy Ξ of 0.79 eV (Table 1). This result confirms the capability of the present Finsler theory to compute the energy of an isolated spherical defect in an externally unloaded volume with reasonable accuracy.

6.4.2. Homogeneous internal structure and comparison with elastic bifurcation

For a homogeneous microstructure, $\xi'(R) = 0 \forall R \in [0, R_0] \Rightarrow \xi(0) = \xi(R_0) = \xi_H$. Boundary conditions on radial displacement $r(R, D) = \varphi(R, D)$ are prescribed as follows:

$$r(0, D) = \varphi_0 = \beta D = \beta l \xi_H, \qquad r(R_0, D) = \varphi_R = a_H R_0 + \beta l \xi_H. \tag{6.57}$$

Here, φ_R is the prescribed outer radius of the deformed sphere, with $a_H = a(R_0)$ and ξ_H constants, and with $\beta \ge 0$ a parameter scaling the radius of a hollow sphere centered at the core of the domain. This hollow sphere physically represents a discrete cavity, while the constant field ξ_H physically represents a continuous distribution of pores or vacancies located throughout the volume. The problem kinematics, with $\xi' = 0$, are consistent with the separable decomposition of the motion φ into

$$\varphi[R, \xi(D)] = \chi(R) + \eta(D) = \chi(R) + \beta l \xi_H, \qquad a = F^r_R = \partial\varphi/\partial R = \mathrm{d}\chi/\mathrm{d}R = \chi'. \tag{6.58}$$

Eqs. (6.40) and (6.50) result in

$$P(R) = (1 - \xi_H)^2 (r^2/R^2) \sigma_1[a(R), r(R), R], \quad (\Upsilon/l)(1 + k\xi_H)\xi_H = (1 - \xi_H)[1 - k(1 - \xi_H)] W_0[a(R), r(R), R]. \tag{6.59}$$

Given φ_R and β as prescribed data, it follows that the second of (6.57) and (6.59) evaluated at $r(R_0) = \varphi_R$ can be solved simultaneously for the homogeneous order parameter field ξ_H, stress $P_H = P(R_0)$, and the radial stretch $a(R_0) = a_H$ at R_0. Then, with ξ_H so determined, (6.58) and (6.59) can be solved simultaneously along $R < R_0$ to determine the distribution of deformation, stress, and resulting energy density inside the sphere. The total energy functional of the elastic sphere with homogeneous internal structure is the volume integral

$$\Psi(\varphi_R, \xi_H) = \Psi_H = 4\pi \int_0^{R_0} \{(1 - \xi_H)^2 W_0[a(R), r(R), R] + \Upsilon \xi_H^2 / l\} R^2 \mathrm{d}R. \tag{6.60}$$

Shown in Fig. 4 are $\xi = \xi_H$, $P(R_0) = P_H$, and average total energy density $\psi_H = \Psi_H/(\frac{4}{3}\pi R_0^3)$ versus applied radial displacement, computed via (6.59) and (6.60). Material parameters correspond to Mg as listed in Table 1, with k varied over a reasonable range as remarked in Section 6.3. Trends are similar to those of Fig. 2: for fixed k, ξ increases monotonically with increasing radial displacement [Fig. 4(a)], radial stress P increases to a maximum and then decreases [Fig. 4(b)], and energy density ψ_H increases monotonically [Fig. 4(c)]. As k increases, ξ tends to decrease for $1.0 < \varphi_R/R_0 < 1.5$, while P and ψ tend to increase. Variations in fields with displacement are qualitatively similar in the present spherical solutions and the shear solutions of Section 5.4.2. Peak radial stress and applied displacement at which peak stress is attained both increase with increasing k, implying an increase in cavitation resistance and stability of the material commensurate with microscopic dilatation represented by $k > 0$. Increases in stress and energy correlate with a decrease in order parameter since both P and strain energy density W are affected by a multiplication factor of $(1 - \xi)^2$ in (6.31) and (6.38). Also shown for comparison in Fig. 4(c) is the elastic energy for the trivial (no cavitation) hyperelastic solution, which can be obtained from the Finsler representation in the limit $\Upsilon/l \to \infty$ or $l \to 0$ such that $\xi_H \to 0$. As physically anticipated, since no defects accommodate expansion, the (elastic) energy exceeds the energy for the other cases when defects nucleate and grow.

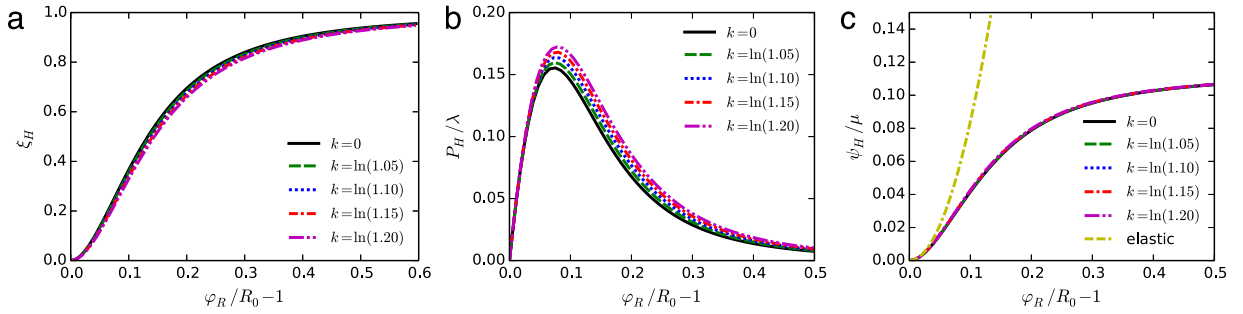

Fig. 4. Spherical deformation, homogeneous solutions, $\beta = 1, l/R_0 = 0.1$ (a) order parameter $\xi = D/l$ (b) normalized radial stress (c) normalized total energy density.

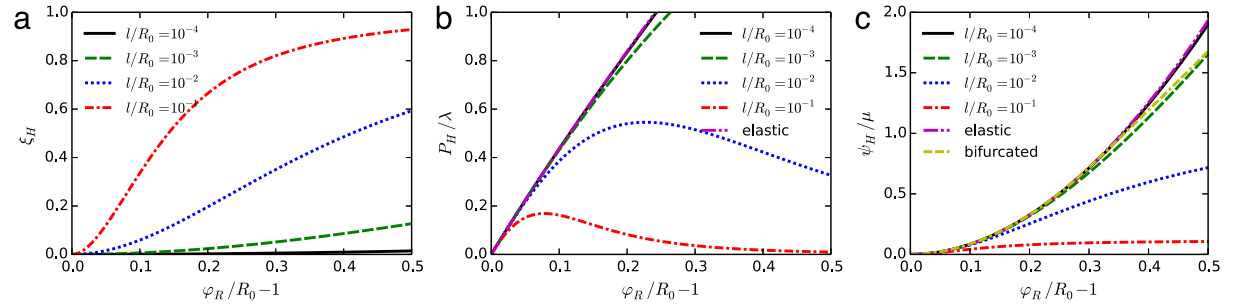

Fig. 5. Spherical deformation, homogeneous solutions, $\exp(k) = 1.16$, $\beta = 1$ (a) order parameter $\xi = D/l$ (b) normalized radial stress (c) normalized total energy density.

Shown in Fig. 5 are order parameter ξ_H, radial stress P_H, and average total energy density ψ_H versus applied radial displacement at fixed $k = \ln(1.16)$. Here, the ratio of regularization length to domain size is varied from 10^{-4} to 10^{-1}. As the regularization length l decreases, microstructure ξ_H grows more slowly with increasing radial displacement at R_0, leading to larger values of radial stress and total energy density relative to cases with larger regularization length. Shown for comparison are stress and energy corresponding to the hyperelasticity solution (i.e., null order parameter) reported in Appendix B, where energies for trivial homogeneous expansion and cavitation to a bifurcated state are computed respectively via (B.9) and (B.12). Note that radial stresses P at R_0 are equal for elastic and bifurcated solutions [92] and are given by (B.8). The classical elastic solution predicts a monotonically increasing radial traction/pressure with increasing applied radial displacement at R_0, regardless of cavity formation. In contrast, the Finsler solution with finite l predicts a radial stress decay after some peak level is attained. The latter trend predicted by the Finsler model is consistent with the response observed in atomic simulations of spherical expansion of crystals; the former is not. Depending on the choice of l and the applied deformation magnitude, the Finsler solution may be more or less energetically stable than the bifurcation solution from nonlinear hyperelasticity, as is evident from Fig. 5(c). Physically, the bifurcated solution corresponds to nucleation and growth of a single discrete cavity at the core of the domain. On the other hand, the homogeneous Finsler solution corresponds to a distribution of vacancies throughout the domain, with a small cavity at the center (for $\beta = 1$ here). The present results thus give the following insight: physically, a material with smaller regularization length l is more likely to undergo discrete cavitation than homogeneous nucleation of vacancies or micro-voids. A larger magnitude of l would suggest a converse stronger tendency towards smeared damage/dilatation mechanisms associated with amorphization.

Effects of variation of the core defect radius, i.e., the factor β in boundary conditions (6.57), on solution variables are shown in Fig. 6, for a relatively small regularization length of $l = 10^{-3}R_0$. For $\beta \leq 10$, the effect of core defect radius is nearly negligible. However, when the radius becomes substantial relative to the domain size, e.g., $\beta = 10^3$, stress and energy become large relative to the other cases, and can even exceed those for the purely hyperelastic solutions at large applied radial displacements. This suggests an energetic tendency for the material to undergo less localized cavitation (i.e., small β preferred) at the expense of distributed dilatation represented by the homogeneous Finsler solutions. The core cavity radius Δ corresponding to Finsler boundary conditions (6.57) is compared with that of the bifurcation solution from neo-Hookean elasticity of Appendix B in Fig. 7. For the former, Δ is negligible by comparison for $\beta \leq 10$, but it is not insignificant for $\beta \geq 100$. The Finsler solution produces a core cavity that grows gradually with applied displacement, while the bifurcation solution predicts rapid cavity growth only after a critical stretch is achieved as quantified in (B.11).

6.4.3. Discussion

Solutions depicted in Fig. 2 demonstrate close agreement of vacancy formation energies among the present theory and experiment [89]. Physically, the generalized pseudo-Finsler theory predicts – upon application of dilatation factor

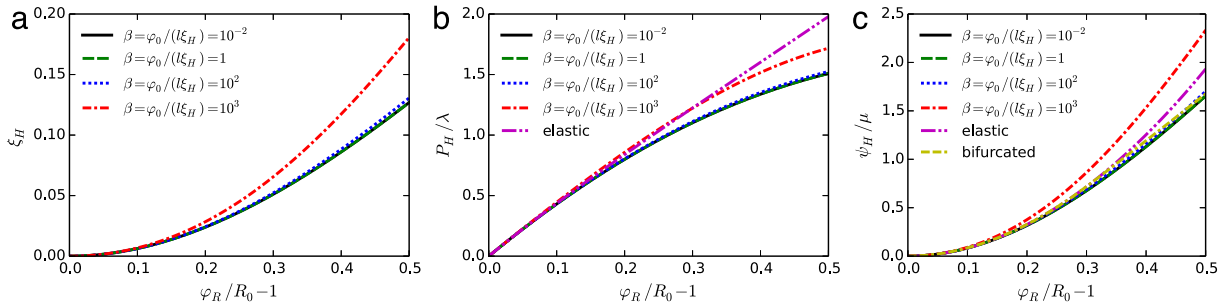

Fig. 6. Spherical deformation, $\exp(k) = 1.16$, $l/R_0 = 10^{-3}$ (a) order parameter $\xi = D/l$ (b) normalized radial stress (c) normalized total energy density.

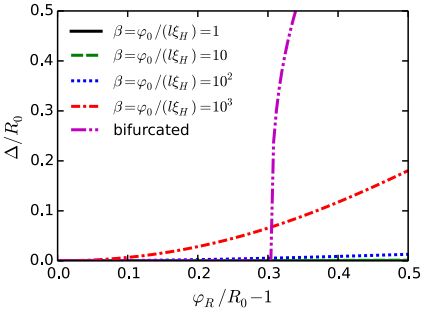

Fig. 7. Spherical deformation, $\exp(k) = 1.16$, $l/R_0 = 10^{-3}$: cavity size $\Delta = \varphi_0 = \beta l\xi_H$ compared to hyperelastic bifurcation solution (B.11).

k motivated by arguments from condensed matter physics (Appendix A and [76]) for a crystalline material undergoing vacancy nucleation and commensurate lattice disordering – a tendency for localized versus distributed cavity formation and growth as regularization length l decreases. A material with smaller regularization length l is more likely to undergo discrete cavitation than homogeneous defect nucleation; a material with larger l is more likely to undergo distributed disordering mechanisms associated with amorphization. Both types of defect mechanisms, i.e., discrete cavitation and distributed lattice dilatation, have been observed in atomic simulations of crystals subjected to far-field boundary conditions of spherical expansion [91]. The discrete cavitation mechanism was found preferable at lower temperatures, while amorphization was found preferable at higher temperatures. Comparison with trends in the present results thus suggests that l could be treated as temperature dependent to reproduce physics observed in atomic simulations; more specifically l should increase with temperature.

It should be noted that the Finsler theory is able to reproduce purely hyperelastic results, and therefore the cavity bifurcation solution, by setting the regularization length l to a very small value, which eliminates the internal structure dependence of the macro-motion and requires, for total energy to remain finite, that the order parameter tends towards a null magnitude. On the other hand, classical nonlinear elasticity lacks the capacity to depict the distributed dilatation and loss of shear stiffness associated with the homogeneous-microstructure solutions of the Finsler theory. In particular, the tensile pressure drop and stiffness reduction observed in atomic simulations [91] cannot be reproduced using the purely elastic solutions of classical elasticity for cavitation given in Appendix B.

7. Conclusions

A new theory, in general considering a deformable vector bundle of pseudo-Finsler character, has been posited, wherein the internal state vector of pseudo-Finsler space is associated with micro-deformation of a material with internal structure. The general objective has been formulation of a physically meaningful theory potentially more descriptive and more predictive than existing models, without incorporation of ad hoc equations or excessive fitting parameters. Rather, the focus has been development of general, and at times more sophisticated, governing equations instead of rudimentary additions to existing model frameworks. It has been demonstrated how this generalized Finsler-geometric theory of continuum mechanics can encompass classes of existing phase field and micromorphic models and subclasses of the latter such as micropolar, second-gradient elasticity, and classical nonlinear elasticity.

Specific problem solutions offer new insight into coupling of microscopic dilatation – captured by a conformal transformation of the metric tensor – with shear failure and cavitation mechanisms in solids. Physically realistic features which are not addressed by other known theories – including phase field and classical and generalized continuum representations – include the following:

- A predicted increase in peak strength with increasing microscopic dilatation in the intensely damaged or localized shearing zone, in agreement with physical observation;
- Prediction of vacancy formation energy, with reasonable accuracy relative to physical experiment, in an unloaded spherical domain with a concentrated defect at its core;
- Solutions to the spherical expansion problem encompassing localized cavity or void formation as well as distributed dilatation associated with transition from a strong dense crystalline to a weakened amorphous or molten state. In these classes of solutions, setting the regularization length to a small value favors the former localized mechanisms over the latter distributed mechanisms.

The general theory seems capable of addressing more diverse physical phenomena in condensed matter depending on differently assumed forms of the fundamental tensor (e.g., anisotropy or directional rescaling) and different sets of connection coefficients, as may be demonstrated in future work.

Acknowledgment

This paper was written while the author served as a visiting research fellow at the Courant Institute of Mathematical Sciences (CIMS) in New York, NY, USA. The author acknowledges the courtesy of Dr. Robert (Bob) Kohn for hosting his sabbatical visit at CIMS in 2016.

Appendix A. Dilatation from point defects

The net volume change from nucleation of a homogeneous density of point defects is computed as follows. The treatment, which is presented in full detail in the monograph [20], pp. 373–378, includes elements from prior work of Eshelby [43] and Teodosiu [62] and the finite deformation geometric framework in [37]. Define $\bar{J} = G^{1/2}$ as the ratio of a spherical volume of material with point defects to that of one without, the latter explicitly with a value of $\frac{4}{3}\pi R_0^3$. Let the number of defects per unit reference volume be ζ, and let the volume fraction of defects be

$$\phi = 1 - \bar{J}^{-1} = \alpha\zeta, \tag{A.1}$$

where α is the net volume change per defect. Assume null traction conditions on the surface of the sphere at $R = R_0$. For nucleation of a vacancy within a volume of fixed mass, the total volume change consists of two competing terms: (i) an increase due to the insertion of the volume of one hole corresponding to a vacated atom and (ii) a decrease due to contraction of this hole associated with local rearrangement of the lattice near the defect core. From [20], eq. (7.104),

$$\alpha = \Omega_0 + (1 + \Gamma)\Delta v, \tag{A.2}$$

where Ω_0 is the atomic volume ($\frac{\sqrt{3}}{4}$a^{2}c for a hexagonal crystal), and the contraction contributions are, from eqs. (7.112) and (7.116) in [20],

$$\Delta v = -c[3\Omega_0\Xi/(2\mu)]^{1/2}, \qquad \Gamma = -(1/c)(\mu' - \mu/K)[2\Xi/(3\mu\Omega_0)]^{1/2}, \tag{A.3}$$

with $c = 3(1-\nu)/(1+\nu)$ a factor depending on Poisson's ratio accounting for the free external surface [43] and with Ξ the vacancy formation energy. Using physical properties for Mg in Table 1, $\alpha = 0.29\Omega_0$.

For application relevant to solutions in Section 6 of this paper, the saturation density of vacancies at which the overall stiffness vanishes (e.g., amorphization or melting) is taken as one vacancy per cell such that $\zeta = \frac{3}{4\pi a^3}$ at $\xi = 1$. Setting $G(\xi) = G(1) = \bar{J}^2 = \exp(2k/3)$ then gives a Weyl scaling factor of $k = \exp(1.16)$. This value is similar to the factor of $k = \exp(1.12)$ corresponding to the volume increase for Mg under shear-induced amorphization/melting in the alternative theoretical treatment of [76].

Appendix B. Solutions for spherical expansion and cavitation: Homogeneous elasticity and bifurcation

Nonlinear elastic solutions presented here and used for comparison of results in Section 6.4.2 follow verbatim from [92], which invokes compressible neo-Hookean elasticity and spherical symmetry. Other treatments have dealt with incompressible nonlinear elasticity and/or symmetry breaking [93–95]. The present solutions involve concepts from classical nonlinear elasticity in the absence of internal structure, e.g., [61]. Radial deformation and its gradient are of the form

$$r = r(R), \qquad a(R) = \mathrm{d}r(R)/\mathrm{d}R = r'(R). \tag{B.1}$$

The problem domain in the undeformed reference state is a sphere of external radius R_0. In physical components, principal stretches are

$$\lambda_1 = a, \qquad \lambda_2 = \lambda_3 = r/R. \tag{B.2}$$

Invariants of the stretch tensor $\sqrt{\boldsymbol{C}}$ in dimensionless physical components [23] are

$$j_1 = \lambda_1 + \lambda_2 + \lambda_3 = a + 2r/R, \qquad j_2 = 1/\lambda_1 + 1/\lambda_2 + 1/\lambda_3 = 1/a + 2R/r, \qquad j_3 = J = \lambda_1\lambda_2\lambda_3 = ar^2/R^2. \quad \text{(B.3)}$$

Strain energy density is linear in each invariant:

$$W_0 = c_1(j_1 - 3) + c_2(j_2 - 3) + c_3(j_3 - 1), \quad \text{(B.4)}$$

where

$$c_1/\mu = (1 - 3\nu)/(1 - 2\nu), \qquad c_2/\mu = (1 - \nu)/(1 - 2\nu), \qquad c_3/\mu = 2\nu/(1 - 2\nu). \quad \text{(B.5)}$$

The trivial solution corresponds to homogeneous deformation, wherein no cavity appears. In this case, boundary conditions on displacement are

$$r(0) = 0; \qquad r(R_0) = \lambda_0 R_0, \qquad \lambda_0 \geq 1. \quad \text{(B.6)}$$

Stretches are equal:

$$\lambda_1 = \lambda_2 = \lambda_3 = a = r/R = \lambda_0, \quad \text{(B.7)}$$

and first Piola–Kirchhoff stress components (e.g., equal radial P and transverse T components) are

$$P = P_r^R = T = RP_\theta^\Theta/r = RP_\phi^\Phi/r = c_1 - c_2/\lambda_0^2 + c_3\lambda_0^2. \quad \text{(B.8)}$$

Total strain energy is

$$\Psi = (4/3)\pi R_0^3(\lambda_0 - 1)^2[3c_2/\lambda_0 + c_3(\lambda_0 + 2)]. \quad \text{(B.9)}$$

The cavitation solution corresponds to formation of a traction-free spherical hole of radius Δ to be computed as an outcome of the loading. In this case, boundary conditions are

$$\lim_{R\to 0^+} r(R) = \Delta > 0, \qquad \lim_{R\to 0^+} P(R) = 0; \qquad r(R_0) = \lambda_0 R_0, \qquad \lambda_0 \geq 1. \quad \text{(B.10)}$$

Cavitation is predicted when $\lambda_0 \geq \lambda_C$, where the applied stretch at bifurcation and the cavity size are [92]

$$\lambda_C = [9c_2/(4c_3)]^{1/4} = [(9/8)(1/\nu - 1)]^{1/4}, \qquad \Delta = \lambda_0 R_0[1 - (\lambda_C/\lambda_0)^2]^{1/3}. \quad \text{(B.11)}$$

First Piola–Kirchhoff stress components cannot be represented in closed form, but radial traction P at $R = R_0$ is identical to that given by the homogeneous solution in (B.8). Total strain energy is

$$\Psi = (4/3)\pi R_0^3[c_1(\alpha_C + 2\lambda_0 - 3) + c_2(1/\alpha_C + 2/\lambda_0 - 3) + c_3(\alpha_C\lambda_0^2 - 1) - (\alpha_C - \lambda_0)(c_1 - c_2/\alpha_C^2 + c_3\lambda_0^2)], \quad \text{(B.12)}$$

where

$$\alpha_C = 2\lambda_0/[3(\lambda_0/\lambda_C)^2 - 1]. \quad \text{(B.13)}$$

For $\lambda_0 < \lambda_C$, no cavity forms, and only the homogeneous solution applies. For $\lambda_0 > \lambda_C$, energy in (B.9) always exceeds that of (B.12), meaning that the cavitation solution is energetically preferable and thus the more stable solution.

References

[1] G. Randers, On an asymmetrical metric in the four-space of general relativity, Phys. Rev. 59 (1941) 195–199.
[2] S. Ikeda, On the theory of fields in Finsler spaces, J. Math. Phys. 22 (1981) 1215–1218.
[3] H. Brandt, Differential geometry of spacetime tangent bundle, Internat. J. Theoret. Phys. 31 (1992) 575–580.
[4] E. Kerner, Extended intertial frames and Lorentz transformations. II, J. Math. Phys. 17 (1976) 1797–1807.
[5] S.-I. Ohta, K.-T. Sturm, Non-contraction of heat flow on Minkowski spaces, Arch. Ration. Mech. Anal. 204 (2012) 917–944.
[6] J. Saczuk, On the role of the Finsler geometry in the theory of elasto-plasticity, Rep. Math. Phys. 39 (1997) 1–17.
[7] P. Finsler, Uber Kurven und Flachen in allgemeiner Raumen, Dissertation, Gottingen, 1918.
[8] E. Cartan, Les Espaces de Finsler, Hermann, Paris, 1934.
[9] S.-S. Chern, Local equivalence and Euclidean connections in Finsler spaces, Sci. Rep. Natl. Tsing Hua Univ. Ser. A 5 (1948) 95–121.
[10] H. Rund, The Differential Geometry of Finsler Spaces, Springer-Verlag, Berlin, 1959.
[11] D. Bao, S.-S. Chern, Z. Shen, An Introduction to Riemann-Finsler Geometry, Springer-Verlag, New York, 2000.
[12] A. Bejancu, H. Farran, Geometry of Pseudo-Finsler Submanifolds, Kluwer, Dordrecht, 2000.
[13] S.-S. Chern, Z. Shen, Riemann-Finsler Geometry, World Scientific, Singapore, 2005.
[14] A. Bejancu, Finsler Geometry and Applications, Ellis Horwood, New York, 1990.
[15] J. Vargas, D. Torr, Finslerian structures: the Cartan-Clifton method of the moving frame, J. Math. Phys. 34 (1993) 4898–4913.
[16] E. Minguzzi, The connections of pseudo-Finsler spaces, Int. J. Geom. Methods Mod. Phys. 11 (2014) 1460025.
[17] S. Amari, A theory of deformations and stresses of ferromagnetic substances by Finsler geometry, in: K. Kondo (Ed.), RAAG Memoirs, vol. 3, Tokyo, 1962, pp. 257–278.
[18] R. Toupin, R. Rivlin, Dimensional changes in crystals caused by dislocations, J. Math. Phys. 1 (1960) 8–15.
[19] J. Wenzelburger, A kinematic model for continuous distributions of dislocations, J. Geom. Phys. 24 (1998) 334–352.
[20] J. Clayton, Nonlinear Mechanics of Crystals, Springer, Dordrecht, 2011.
[21] K. Le, H. Stumpf, On the determination of the crystal reference in nonlinear continuum theory of dislocations, Proc. R. Soc. Lond. Ser. A Math. Phys. Eng. Sci. 452 (1996) 359–371.
[22] J. Clayton, On anholonomic deformation, geometry, and differentiation, Math. Mech. Solids 17 (2012) 702–735.

[23] J. Clayton, Differential Geometry and Kinematics of Continua, World Scientific, Singapore, 2014.
[24] K. Kondo, Non-holonomic foundations of the theory of plasticity and yielding, in: K. Kondo (Ed.), RAAG Memoirs, vol. 1, Tokyo, 1955, pp. 522–562.
[25] K. Kondo, Non-Riemannian and Finslerian approaches to the theory of yielding, Internat. J. Engrg. Sci. 1 (1963) 71–88.
[26] E. Kröner, Interrelations between various branches of continuum mechanics, in: E. Kröner (Ed.), Mechanics of Generalized Continua, Springer, Berlin, 1968, pp. 330–340.
[27] A. Eringen, in: A. Eringen (Ed.), Tensor Analysis, in: Continuum Physics, vol. I, Academic Press, New York, 1971, pp. 1–155.
[28] S. Ikeda, A geometrical construction of the physical interaction field and its application to the rheological deformation field, Tensor (N.S.) 24 (1972) 60–68.
[29] S. Ikeda, A physico-geometrical consideration on the theory of directors in the continuum mechanics of oriented media, Tensor (N.S.) 27 (1973) 361–368.
[30] J. Saczuk, Finslerian Foundations of Solid Mechanics, Polskiej Akademii Nauk, Gdansk, 1996.
[31] H. Stumpf, J. Saczuk, A generalized model of oriented continuum with defects, ZAMM Z. Angew. Math. Mech. 80 (2000) 147–169.
[32] T. Yajima, H. Nagahama, Finsler geometry of seismic ray path in anisotropic media, Proc. R. Soc. Lond. Ser. A Math. Phys. Eng. Sci. 465 (2009) 1763–1777.
[33] J. Clayton, On Finsler geometry and applications in mechanics: review and new perspectives, Adv. Math. Phys. 828475.
[34] W. Noll, Materially uniform simple bodies with inhomogeneities, Arch. Ration. Mech. Anal. 27 (1967) 1–32.
[35] C.-C. Wang, On the geometric structures of simple bodies, a mathematical foundation for the theory of continuous distributions of dislocations, Arch. Ration. Mech. Anal. 27 (1967) 33–94.
[36] J. Marsden, S. Pekarsky, S. Shkoller, M. West, Variational methods, multisymplectic geometry and continuum mechanics, J. Geom. Phys. 38 (2001) 253–284.
[37] J. Clayton, D. Bammann, D. McDowell, A geometric framework for the kinematics of crystals with defects, Phil. Mag. 85 (2005) 3983–4010.
[38] J. Clayton, Defects in nonlinear elastic crystals: differential geometry, finite kinematics, and second-order analytical solutions, ZAMM Z. Angew. Math. Mech. 95 (2015) 476–510.
[39] P. Steinmann, Geometrical Foundations of Continuum Mechanics, Springer, Berlin, 2015.
[40] J. Clayton, J. Knap, Nonlinear phase field theory for fracture and twinning with analysis of simple shear, Phil. Mag. 95 (2015) 2661–2696.
[41] W. Brace, B. Paulding, C. Scholz, Dilatancy in the fracture of crystalline rocks, J. Geophys. Res. 71 (1966) 3939–3953.
[42] J. Clayton, Deformation, fracture, and fragmentation in brittle geologic solids, Int. J. Fract. 163 (2010) 151–172.
[43] J. Eshelby, Distortion of a crystal caused by point imperfections, J. Appl. Phys. 25 (1954) 255–261.
[44] J. Clayton, An alternative three-term decomposition for single crystal deformation motivated by non-linear elastic dislocation solutions, Q. J. Mech. Appl. Math. 67 (2014) 127–158.
[45] H. Weyl, Space-Time-Matter, fourth ed., Dover, New York, 1952.
[46] V. Canuto, P. Adams, S.-H. Hsieh, E. Tsiang, Scale-covariant theory of gravitation and astrophysical applications, Phys. Rev. D 16 (1977) 1643–1663.
[47] A. Ozakin, A. Yavari, A geometric theory of thermal stresses, J. Math. Phys. 51 (2010) 032902.
[48] J. Clayton, D. McDowell, A multiscale multiplicative decomposition for elastoplasticity of polycrystals, Int. J. Plast. 19 (2003) 1401–1444.
[49] J. Clayton, Dynamic plasticity and fracture in high density polycrystals: constitutive modeling and numerical simulation, J. Mech. Phys. Solids 53 (2005) 261–301.
[50] R. Kohn, The relaxation of a double-well energy, Contin. Mech. Thermodyn. 3 (1991) 193–236.
[51] H. Rund, A divergence theorem for Finsler metrics, Monatsh. Math. 79 (1975) 233–252.
[52] G. Capriz, Continua with Microstructure, Springer, New York, 1989.
[53] C. Fabritiis, P. Mariano, Geometry of interactions in complex bodies, J. Geom. Phys. 54 (2005) 301–323.
[54] R. Toupin, Theories of elasticity with couple stress, Arch. Ration. Mech. Anal. 17 (1964) 85–112.
[55] R. Mindlin, Microstructure in linear elasticity, Arch. Ration. Mech. Anal. 16 (1964) 51–78.
[56] J. Clayton, J. Knap, A phase field model of deformation twinning: nonlinear theory and numerical simulations, Physica D 240 (2011) 841–858.
[57] A. Hushmandi, M. Rezaii, On the curvature of warped product Finsler spaces and the Laplacian of the Sasaki-Finsler metrics, J. Geom. Phys. 62 (2012) 2077–2098.
[58] J. Li, The variation formulas of Finsler submanifolds, J. Geom. Phys. 61 (2011) 890–898.
[59] P. Grinfeld, Introduction to Tensor Analysis and the Calculus of Moving Surfaces, Springer, New York, 2013.
[60] C. Truesdell, R. Toupin, in: S. Flugge (Ed.), The Classical Field Theories, in: Handbuch der Physik, vol. III/1, Springer-Verlag, Berlin, 1960, pp. 226–793.
[61] R. Ogden, Non-linear Elastic Deformations, Ellis Horwood, Chichester, 1984.
[62] C. Teodosiu, Elastic Models of Crystal Defects, Springer, Berlin, 1982.
[63] A. Kholodenko, Use of quadratic differentials for description of defects and textures in liquid crystals and 2 + 1 gravity, J. Geom. Phys. 33 (2000) 59–102.
[64] M. Grinfeld, Thermodynamic Methods in the Theory of Heterogeneous Systems, Longman Scientific and Technical, Sussex, 1991.
[65] R. Segev, E. Fried, G. DeBotton, Force theory for multiphase bodies, J. Geom. Phys. 20 (1996) 371–392.
[66] J. Clayton, P. Chung, An atomistic-to-continuum framework for nonlinear crystal mechanics based on asymptotic homogenization, J. Mech. Phys. Solids 54 (2006) 1604–1639.
[67] W. E, P. Ming, Cauchy-Born rule and the stability of crystalline solids: static problems, Arch. Ration. Mech. Anal. 183 (2007) 241–297.
[68] V. Levitas, V. Levin, K. Zingerman, E. Freiman, Displacive phase transitions at large strains: phase-field theory and simulations, Phys. Rev. Lett. 103 (2009) 025702.
[69] S. Allen, J. Cahn, A microscopic theory for antiphase boundary motion and its application to antiphase domain coarsening, Acta Metall. 27 (1979) 1085–1095.
[70] P. Yu, S.Y. Hu, L.Q. Chen, Q. Du, An iterative-perturbation scheme for treating inhomogeneous elasticity in phase-field models, J. Comput. Phys. 208 (2005) 34–50.
[71] T. Wright, The Physics and Mathematics of Adiabatic Shear Bands, Cambridge University Press, Cambridge, 2002.
[72] D. Curran, L. Seaman, T. Cooper, D. Shockey, Micromechanical model for comminution and granular flow of brittle material under high strain rate application to penetration of ceramic targets, Int. J. Impact Eng. 13 (1993) 53–83.
[73] M. Rist, High-stress ice fracture and friction, J. Phys. Chem. 101 (1997) 6263–6266.
[74] J. Holder, A. Granato, Thermodynamic properties of solids containing defects, Phys. Rev. 182 (1969) 729–741.
[75] A. Korbel, V. Raghunathan, D. Teirlinck, W. Spitzig, O. Richmond, J. Embury, A structural study of the influence of pressure on shear band formation, Acta Metall. 32 (1984) 511–519.
[76] F. Delogu, Connection between shear instability and amorphisation, Mater. Sci. Eng. 367 (2004) 162–165.
[77] J. Simo, K. Pister, Remarks on rate constitutive equations for finite deformation problems: computational implications, Comput. Methods Appl. Mech. Engrg. 46 (1984) 201–215.
[78] J. Clayton, J. Knap, Phase field modeling of twinning in indentation of transparent single crystals, Modelling Simul. Mater. Sci. Eng. 19 (2011) 085005.
[79] J. Clayton, J. Knap, Phase field analysis of fracture induced twinning in single crystals, Acta Mater. 61 (2013) 5341–5353.
[80] J. Clayton, K. Bliss, Analysis of intrinsic stability criteria for isotropic third-order Geen elastic and compressible neo-Hookean solids, Mech. Mater. 68 (2014) 104–119.
[81] B. Bourdin, G. Francfort, J. Marigo, The variational approach to fracture, J. Elasticity 91 (2008) 5–148.
[82] M. Borden, C. Verhoosel, M. Scott, T.. Hughes, C. Landis, A phase-field description of dynamic brittle fracture, Comput. Methods Appl. Mech. Engrg. 217 (2012) 77–95.
[83] M. Yoo, Slip, twinning, and fracture in hexagonal close-packed metals, Metall. Trans. A 12 (1981) 409–418.
[84] R. Hearmon, The elastic constants of anisotropic materials, Rev. Mod. Phys. 18 (1946) 409–439.

[85] J. Rice, Mathematical analysis in the mechanics of fracture, in: H. Liebowitz (Ed.), Fracture: An Advanced Treatise, Academic Press, New York, 1968, pp. 191–311.
[86] J. Clayton, R. Kraft, R. Leavy, Mesoscale modeling of nonlinear elasticity and fracture in ceramic polycrystals under dynamic shear and compression, Int. J. Solids Struct. 49 (2012) 2686–2702.
[87] B. Kondori, A. Benzerga, Effect of stress triaxiality on the flow and fracture behavior of Mg alloy AZ31, Metall. Mater. Trans. A 45 (2014) 3292–3307.
[88] M. Guinan, D. Steinberg, Pressure and temperature derivatives of the isotropic polycrystalline shear modulus for 65 elements, J. Phys. Chem. Solids 35 (1974) 1501–1512.
[89] P. Tzanetakis, J. Hillairet, G. Revel, The formation energy of vacancies in aluminium and magnesium, Phys. Status Solidi b 75 (1976) 433–439.
[90] W. Nixon, E. Schulson, A micromechanical view of the fracture toughness of ice, J. Physique 48 (1997) C313–C319.
[91] J. Wang, S. Yip, S. Phillpot, D. Wolf, Intrinsic response of crystals to pure dilatation, J. Alloys Compd. 194 (1993) 407–415.
[92] S. Chun, C. Jun, Exact solution for cavitated bifurcation for compressible hyperelastic materials, Internat. J. Engrg. Sci. 39 (2001) 1101–1117.
[93] J. Ball, Discontinuous equilibrium solutions and cavitation in nonlinear elasticity, Philos. Trans. R. Soc. Lond. Ser. A Math. Phys. Eng. Sci. 306 (1982) 557–611.
[94] H. Abeyaratne, H. Hou, On the occurrence of the cavitation instability relative to the asymmetric instability under symmetry dead-loading conditions, Q. J. Mech. Appl. Math. 44 (1991) 429–449.
[95] V.A. Eremeyev, L. Zubov, M. Kariakin, N. Chernega, Formation of cavities in nonlinearly elastic bodies with dislocations and disclinations, Dokl. Akad. Nauk Minerologia USSR 326 (1992) 968–971.